Quaternary Science Reviews 157 (2017) 29–51

Contents lists available at ScienceDirect

Quaternary Science Reviews

journal homepage: www.elsevier.com/locate/quascirev

Atlantic forcing of Western Mediterranean winter rain minima during the last 12,000 years

Christoph Zielhofer [a, *], William J. Fletcher [b], Steffen Mischke [c], Marc De Batist [d], Jennifer F.E. Campbell [b], Sebastien Joannin [e], Rik Tjallingii [f], Najib El Hamouti [g], Annett Junginger [h], Andreas Stele [i], Jens Bussmann [i], Birgit Schneider [a], Tobias Lauer [a, j], Katrin Spitzer [k], Michael Strupler [l], Thomas Brachert [m], Abdeslam Mikdad [n]

[a] Institute of Geography, Leipzig University, Leipzig, Germany
[b] School of Environment and Development, University of Manchester, Manchester, United Kingdom
[c] Faculty of Earth Sciences, University of Iceland, Reykjavik, Iceland
[d] Renard Centre of Marine Geology, Ghent University, Ghent, Belgium
[e] Institut des Sciences de l'Evolution, Montpellier University, France
[f] GFZ German Research Centre for Geosciences, Section 5.2 – Climate Dynamics and Landscape Evolution, Potsdam, Germany
[g] Faculté Pluridisciplinaire Nador, Université Mohamed I Oujda, Morocco
[h] Faculty of Geosciences, Tübingen University, Germany
[i] Institute of Geography, Osnabruck University, Osnabruck, Germany
[j] Max Planck Institute for Evolutionary Anthropology, Department of Human Evolution, Leipzig, Germany
[k] Institute of Geological Sciences, Freie Universität Berlin, Berlin, Germany
[l] Department of Earth Sciences, ETH Zurich, Switzerland
[m] Institute of Geophysics and Geology, Leipzig University, Leipzig, Germany
[n] Institut National des Sciences de l'Archéologie et du Patrimoine, Rabat, Morocco

ARTICLE INFO

Article history:
Received 21 October 2015
Received in revised form
22 September 2016
Accepted 29 November 2016
Available online 19 December 2016

Keywords:
Holocene
Younger Dryas
Winter rain minima
Atlantic forcing
Western Mediterranean
North Atlantic Oscillation (NAO)
Seasonality
Solar forcing
Lake sediments
Middle Atlas
Morocco

ABSTRACT

The limited availability of high-resolution continuous archives, insufficient chronological control, and complex hydro-climatic forcing mechanisms lead to many uncertainties in palaeo-hydrological reconstructions for the Western Mediterranean. In this study we present a newly recovered 19.63 m long core from Lake Sidi Ali in the North African Middle Atlas, a transition zone of Atlantic, Western Mediterranean and Saharan air mass trajectories. With a multi-proxy approach based on magnetic susceptibility, carbonate and total organic C content, core-scanning and quantitative XRF, stable isotopes of ostracod shells, charcoal counts, *Cedrus* pollen abundance, and a first set of diatom data, we reconstruct Western Mediterranean hydro-climatic variability, seasonality and forcing mechanisms during the last 12,000 yr. A robust chronological model based on AMS ^{14}C dated pollen concentrates supports our high-resolution multi-proxy study. Long-term trends reveal low lake levels at the end of the Younger Dryas, during the mid-Holocene interval 6.6 to 5.4 cal ka BP, and during the last 3000 years. In contrast, lake levels are mostly high during the Early and Mid-Holocene. The record also shows sub-millennial- to centennial-scale decreases in Western Mediterranean winter rain at 11.4, 10.3, 9.2, 8.2, 7.2, 6.6, 6.0, 5.4, 5.0, 4.4, 3.5, 2.9, 2.2, 1.9, 1.7, 1.5, 1.0, 0.7, and 0.2 cal ka BP. Early Holocene winter rain minima are in phase with cooling events and millennial-scale meltwater discharges in the sub-polar North Atlantic. Our proxy parameters do not show so far a clear impact of Saharan air masses on Mediterranean hydro-climate in North Africa. However, a significant hydro-climatic shift at the end of the African Humid Period (~5 ka) indicates a change in climate forcing mechanisms. The Late Holocene climate variability in the Middle Atlas features a multi-centennial-scale NAO-type pattern, with Atlantic cooling and Western Mediterranean winter rain maxima generally associated with solar minima.

* Corresponding author.
E-mail address: zielhofer@uni-leipzig.de (C. Zielhofer).

http://dx.doi.org/10.1016/j.quascirev.2016.11.037

1. Introduction

Western Mediterranean environments are considered some of the most sensitive landscapes to global warming (Giorgi, 2006). Future climate changes in the Western Mediterranean region will enhance the occurrence of heat stress (Diffenbaugh et al., 2007) and droughts (Born et al., 2008) and will reduce mean annual precipitation (Solomon et al., 2009). In order to refine scenarios for future climate changes it is important to integrate palaeoclimatic data in climatic models (Flato et al., 2013). On this note, high-resolution continuous palaeoclimatic data from recovered lake sediments allow the reconstruction of past climatic oscillations and cycles on decadal- to millennial timescales (Corella et al., 2014). Furthermore, the compilation of continuous palaeoenvironmental proxy-data is a tool for reconstructing shifts and thresholds of natural landscape systems in response to gradual and rapid climatic forcing (Roberts et al., 2011; Fletcher and Zielhofer, 2013).

While Holocene global Rapid Climate Changes (RCCs) are generally characterised by cooling (Mayewski et al., 2004), regional to sub-regional changes in precipitation pattern appear to be much more important in the Western Mediterranean for environmental change. Evidence from numerous records points to perturbation of the Western Mediterranean hydrological regime during the Holocene. Geomorphological, palaeohydrological and palaeoecological records indicate hydro-climatic impacts on vegetation (Fletcher et al., 2013; Nourelbait et al., 2014), lake levels (Lamb et al., 1995; Pérez-Sanz et al., 2013), fire regimes (Linstädter and Zielhofer, 2010; Reddad et al., 2013), fluvial dynamics (Zielhofer et al., 2010; Wolf and Faust, 2015) and aeolian sediment mobilisation (Bout-Roumazeilles et al., 2013). While it is already challenging to link phases of aridity and humidity on a sub-regional to regional scale (Carrión, 2002; Benito et al., 2015), the reconstruction of past Mediterranean hydro-climate becomes more complex by integrating varying seasonality (Lamb et al., 1995).

Current studies and reviews of Holocene palaeoclimatic changes at continental scales of the Atlantic realm mainly focus on temperate (Magny et al., 2012; Moreno et al., 2014a) or monsoonal (Shanahan et al., 2015) air mass variability. However, there is only scarce knowledge of hydro-climatic interaction at the Northern Saharan desert margin, a zone of transition with current impacts of Atlantic, Western Mediterranean and Saharan air masses. Well-dated and high-resolution studies of the palaeoenvironmental evolution of the Middle Atlas mountainous desert margin are required to understand climatic interactions in this zone.

Despite pioneering palaeolimnological works in the Middle Atlas (El Hamouti, 1991, Barker et al., 1994; Lamb et al., 1995, 1999; Lamb and van der Kaars, 1995; Cheddadi et al., 1998) and recent palaeoenvironmental studies (e.g. Nourelbait et al., 2014, 2015) including a focus on anthropogenic impacts (Cheddadi et al., 2015), there remains a need for continuous records with robust chronologies in Mediterranean North Africa, which allow a clear coupling with continuous climatic archives in the wider region. For example, while Lamb et al. (1995) detect sub-millennial-scale impacts of Atlantic air masses on the Holocene hydro-climate in Mediterranean North Africa, the forcing mechanisms (Fletcher et al., 2013), timing, and impacts on Western Mediterranean environments (McGregor et al., 2009) are still under debate.

The aim of this study is the reconstruction of the centennial-scale hydro-climatic history of the Middle Atlas as a mountainous Saharan desert margin based on a stratigraphical multi-proxy approach and a hydrological sampling program at Lake Sidi Ali. We aim to develop a pollen-based ^{14}C chronology to reduce hard-water induced errors in radiocarbon dating of lacustrine sediments and to create the most robust terrestrial chronology for Morocco and of relevance to the Western Mediterranean in a broader scale. The approach should yield insights into orbital-, sub-millennial and centennial-scale climatic variability of the Western Mediterranean at its zone of transition towards the Sahara in the South, including evaluation of the role of climatic forcing by North Atlantic cooling episodes, ice-rafting (Bond events) and solar variability. The study aims to trace shifting impacts of Atlantic, Mediterranean and southern air mass trajectories and to gain knowledge about their variability, seasonality and forcing mechanisms. This knowledge is ultimately valuable for extending the understanding of key modes of climatic variability, such as the North Atlantic Oscillation (NAO), beyond the limits of historical and tree-ring records (Trouet et al., 2009).

2. Geographical setting

Lake Sidi Ali (33° 03′N, 5° 00′W, 2080 m a.s.l.) is located in the Middle Atlas, Morocco (Fig. 1a). The lake lies in a depression of structural origin along a fault-line between Middle Jurassic limestone in the south-east and Lower Jurassic dolomite in the north-west (Fig. 1b). The northern boundary of Lake Sidi Ali is prescribed by the Plio-Pleistocene Sidi Ali volcano. The catchment includes mountains reaching 2220–2338 m. The surrounding forest vegetation of evergreen oak (*Quercus rotundifolia*) and Atlantic cedar (*Cedrus atlantica*) is representative of the montane Mediterranean bioclimatic zone but degraded due to overgrazing.

The lake lies within a small, closed catchment of approx. 14 km^2 and has a varying surface between 2.0 and 2.8 km^2 due to high sensitivity with respect to changes in precipitation/evaporation balance (Sayad et al., 2011). Depending on water level fluctuations, the lake may be separated in two sub-basins by a basalt ridge, as it has been since 1974 (Barker et al., 1994). Previous research on the southern shallow sub-lake (Barker et al., 1994; Lamb et al., 1999) indicates a minimum sediment depth of 635 cm covering a time-span from 0 to 7 cal ka BP. The main lake (Fig. 1b) was never drilled before from a raft.

The mean annual precipitation (1982–2009) is 430 mm at Lake Sidi Ali. The dry season lasts from June to September and the wet period from October to May (Fig. 1c). The position of the lake is within a strong N-S hydrological gradient and reflects a mountainous desert margin between the sub-humid Mediterranean climate in the north and the arid to semiarid High Atlas in the south (Linstädter and Zielhofer, 2010). The mean annual temperature is 10.3 °C with a minimum in January of 2.0 °C and a maximum in July of 19.7 °C.

3. Methods

3.1. Bathymetric and acoustic sub-bottom profiling

Lake Sidi Ali was surveyed in September 2012 with a high-resolution acoustic system (pinger with 3.5 kHz central frequency) mounted on a cataraft attached on the side of a motorized raft (cruising speed 3.5 knots). The data were acquired and processed with DELPH Seismic Acquisition Software (IXBLUE) and interpreted with IHS Kingdom 8.7 Software. For the calculation of water depths, a p-wave velocity of 1500 m/s was used. Bathymetric and seismic data were used to create a bathymetric map, to investigate the stratigraphy of the lake infills and to inform the positioning of coring site.

3.2. Hydrological analyses

A hydrological survey was also undertaken in September 2012, sampling streams and springs in the vicinity of the lake (Fig. 1b). At each sampling locality, pH value, specific conductivity and oxygen

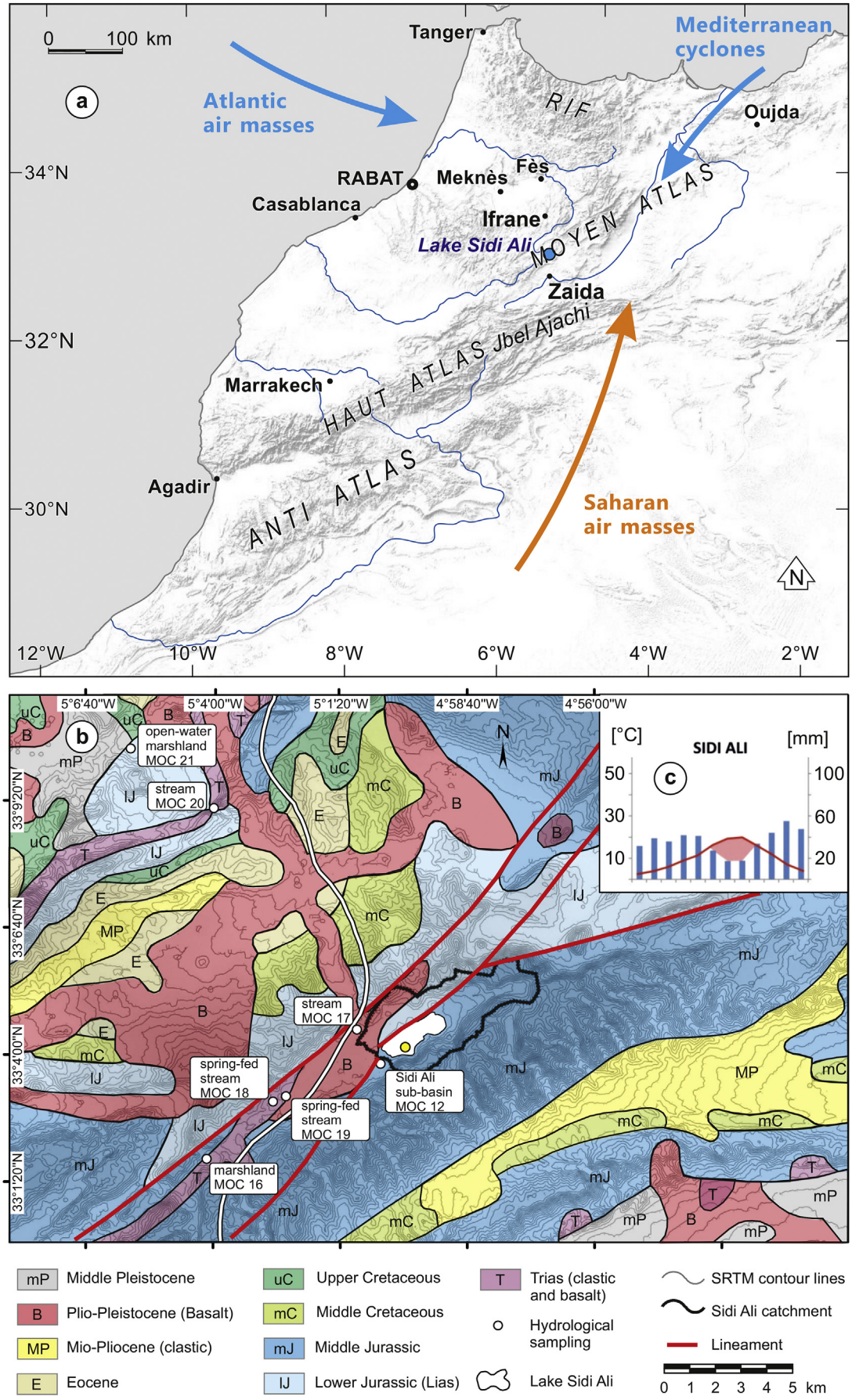

Fig. 1. Geographical, geological and climatological setting of Lake Sidi Ali, showing: a) location of the lake in the Moroccan Middle Atlas (Moyen Atlas), with the hypothetical impact of different air masses on Holocene climate history indicated by arrows; b) geological map of the surrounding area of Sidi Ali showing principal geological units, lineaments and hydrological sampling sites; geological data are derived from Saadi et al. (1985); drilling position is located with a yellow dot; and c) Sidi Ali climate chart (data courtesy of l'Agence du Bassin Hydraulique du Sebou).

saturation were directly measured on site. Major ion concentrations were subsequently measured with a Dionex ion chromatograph DX 120 after filtration with a 0.45 μm cellulose acetate filter. The hydrogen and oxygen isotope composition of water samples were measured with a PICARRO L2130i Isotopic Water Liquid Analyser using Cavity Ring-Down Spectroscopy (CRDS). For each sample, six repeat measurements were conducted (Meyer et al., 2000). The external errors of long-term standard measurements for H and O isotope composition are ±0.8‰ and ±0.1‰, respectively. A hydro-chemical water-depth profile at the maximum water-depth of Lake Sidi Ali was taken (Fig. 2). Electrical conductivity, pH and oxygen saturation were measured directly on site in 1 m intervals using 40 m sensor cables.

3.3. Drilling program and magnetic susceptibility record

A new core was recovered at the deepest position of the lake (33° 4′ 4.908″N, 4° 59‘ 50.640″W) in a zone of undisturbed

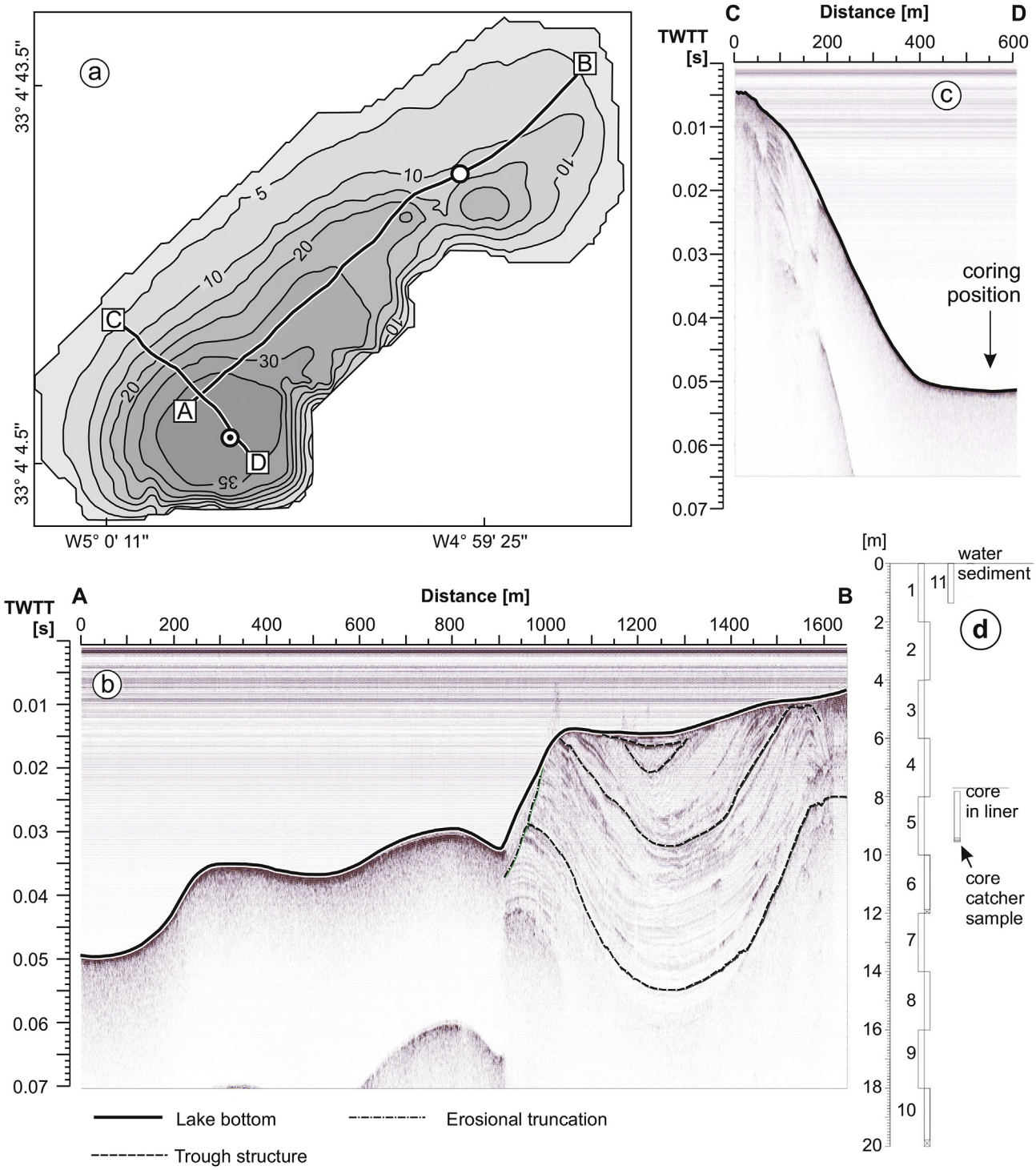

Fig. 2. Results of bathymetric and seismic surveys, showing: a) Sidi Ali bathymetric map with drilling position and sampling site for the water-depth profile; AB and CD black lines represent the positions of seismic profiles; b) AB seismic profile; c) CD seismic profile with drilling position; and d) Sidi Ali core recovery (Ali 1 to 10 and Ali 11).

stratigraphy from a floating platform (Figs. 1b and 2d, Ali 1 to 10 core sections) using a UWITEC piston corer with a 2 m core chamber fitted with 59 mm diameter PVC liners. The total drilling depth was determined by the capability of the coring system, not the depth of infill. An additional Ali 11 short core was also recovered using a UWITEC gravity corer (Fig. 2d). Volume magnetic susceptibility of the cores in plastic-liners was determined in the field using the Bartington MS2C core logging sensor. Measurement intervals were set to 2 cm.

3.4. Splitting, visual description and sub-sampling

The cores were split longitudinally into two halves, photographed and stratigraphically described (Table 1). Wet sediment colour was determined using a Munsell Soil Colour Chart. Visible plant remains (wood, charcoal) and mollusc shells were noted.

3.5. Carbonate content and TOC content

Total organic carbon (TOC) was measured using an Elementar CNS analyser vario EL cube and total inorganic carbon (TIC) determined by Scheibler carbonate measurements.

3.6. XRF analyses

Bulk samples from the recovered cores were analysed with a Spectro Xepos X-ray fluorescence device. For XRF sample preparation air-dried bulk sediment (4 g) was sieved (2 mm). Subsequently a homogenization of the sample was undertaken with a vibratory Retsch mill MM 200. Pressed pellets were prepared using a Vaneox press at 20 t for 2 min. Measurements were conducted in a He atmosphere. K, Fe, Ti contents are used as a proxy for detrital sediment components (Kylander et al., 2011). Split core halves were analysed every 1 mm with an ITRAX XRF core scanner to obtain a high-resolution Ca record (Croudace et al., 2006). The Ca intensities obtained by the XRF scanning were calibrated using TOC and TIC measurements on discrete samples using a multivariate log-ratio calibration model.

3.7. Diatom analyses

A first sampling for diatoms was conducted at 100 cm intervals (following El Hamouti, 2003). The observation of the slides was carried out under the optical microscope (×1000). The relative frequency of a species was calculated after counting of at least 300 valves. Diatom species were determined following El Hamouti (2014) and Anderson et al. (2015). The taxonomic delimitation of some Middle Atlas *Cyclotella* taxa is difficult due to the polymorphism of the valves. Hence, an open taxonomy is adopted for those diatoms, which do not fit precisely to any defined taxa. This is the case for Cyclotella sp. aff. *comensis* type 3, *Cyclotella* sp. aff. *comensis* type 1, and for *Cyclotella* sp. aff. *ocellata* type 4 (El Hamouti, 2003, 2014).

Following Barker et al. (1994) we compute the Planktonic/Littoral ratio (P/L) as a proxy for lake level changes at Sidi Ali. The planktonic *Cyclotella* sp. aff. *comensis* type 3 (Fig. 7a), *Cyclotella parva* (Fig. 7b), *Cyclotella azigzensis* (Fig. 7c and Fig. A2a), *Cyclotella* sp. aff. *comensis* type 1 (Fig. 7e), *Stephanodiscus* spp., and *Melosira granulata* are considered here. *Cyclotella* sp. aff. *ocellata* type 4 (Fig. 7d) and *Fragilaria* spp. (predominantly *Fragilaria brevistriata*) (Fig. 7f) are not considered here, as these species do not clearly represent fully pelagic conditions (Flower et al., 1989; Barker et al., 1994; El Hamouti, 2003, 2014). The P/L ratio considers fully epiphytic and/or littoral species as littoral life-forms. The relative sum of diatom species with ecological optima above 3.2 mS/cm (*Amphora pediculus*, *Amphora veneta*, *Achnanthes affinis*, *Surirella ovalis*, *Pleurosigma* sp., *Mastogloia smithïi*, *Navicula oblongo*, *Navicula halophila*, *Navicula radiosa*, *Navicula rhynchocephala* according to Gasse et al., 1995) is considered as a lake salinity proxy.

3.8. Ostracod and macro-charcoal analyses

Freeze-dried sub-samples of 8 g were treated with 3% H_2O_2 for four days and sieved with 100 and 250 μm meshes. Sieve residues were checked for ostracods and macro-charcoal remains using a low-power binocular microscope. Up to 300 adult ostracod shells were picked per sample. If fewer than 300 adult ostracod shells were found in a sample, both adult and juvenile shells were collected. Ostracods (Fig. A1) are predominantly benthic dwellers and were mainly identified based on Meisch (2000). Macro-charcoal remains were counted from both sieve residual fractions. The abundance of the large diatom *Campylodiscus clypeus* in sieve residues was assessed using a four-step semi-quantitative scale.

3.9. C and O stable isotopes of ostracod shells

About 20 μg of adult ostracod shell material from the closely related species *Fabaeformiscandona* sp. and *Candona* sp. were used

Table 1
Sedimentological units – qualitative summary of sediment zone characteristics.

Unit	Depth (cm)	Structure	Bedding scale	Colour and colour changes	CO_3 [%]	TOC [%]	Mag. Susc. [10^{-6} SI]	Sulfur	Internal variability (frequency)	Internal variability (magnitude)
5	0–435	Faint horizontal bedding	cm to sub-cm	2.5 Y 3/1 to 4/2, gradual	Mid 20–40	Low 7–12	High 50–120	Low	High	High, peaks in MS vs TOC
4c	435–955	Faint horizontal bedding	sub-cm to mm	5 Y 3/2 to 2.5 Y 2.5/1, gradual	High ~40	Mid 12–15	Mid 40–60	High/variable	Mid	Low, peaks in MS + CO_3 vs TOC
4b	955–1150	Faint horizontal bedding	cm to sub-cm	2.5 Y 3/2 to 10 YR 2/2, gradual	Mid 20–40	High 13–18	Mid 40–60	High/variable	Mid	Moderate, peaks in MS + CO_3 vs TOC
4a	1150–1320	Faint horizontal bedding	cm to sub-cm	2.5 Y 2.5/1 to 3/2, gradual	High ~30	Low 10–15	High 50–75	Low	Mid	High, peaks in MS + CO_3 vs TOC
3	1320–1640	Faint horizontal bedding	sub-cm to mm	Alternation of lighter (2.5 Y 3/2) and darker (10 YR 2/2) sub-zones, gradual changes	Low 10–20	High ~15	Low <40	Mid	Mid	High, peaks in MS + CO_3 vs TOC
2	1640–1815	Faint horizontal bedding	sub-cm to mm	2.5 Y 2.5/1 to 4/2, gradual	Mid 20–25	Mid 12–14	Low <40	Mid	Low	Low
1	1815–1963	Faint horizontal bedding	sub-cm to mm	2.5 Y 4/2, very slight gradual changes	High 30–40	Low ~10	Low <40	Low	Low	Low

for C and O stable isotope analyses. The ecology and life cycle of the two species is not known but formation of shells probably occurs sometime during the warm season due to the cold setting of the lake. If adult shells were not sufficiently present in a sample, shells of latest instars were used. Shells were reacted with 105% phosphoric acid at 70 °C using a Kiel IV online carbonate preparation line connected to a MAT 253 mass spectrometer. All carbonate values are reported in ‰ relative to VPDB according to the delta notation. Reproducibility was checked by replicate analysis of NBS19 and was better than ±0.02‰ (1σ) for $\delta^{13}C$ and better than ±0.06‰ (1σ) for $\delta^{18}O$ values.

3.10. Pollen analyses

Pollen samples were prepared at 10 cm intervals using a combination of the standard HF and acetolysis procedure (Moore et al., 1991), in combination with dense media separation (Nakagawa et al., 1998) using sodium polytungstate (SPT) and sieving at 180 μm. Residues were mounted on slides with silicon oil and a minimum of 300 terrestrial grains were counted under high power (400×/1000×) magnification.

3.11. ^{210}Pb and ^{137}Cs dating and ^{14}C dating of pollen concentrates

^{210}Pb and ^{137}Cs dating procedures were applied to 1-cm thick samples from Ali 11 core (Appleby et al., 1986, 1992). We transferred the Ali 11 chronological information from ^{210}Pb, ^{137}Cs and ^{14}C radiometric dating to Ali 1 core by the matching of 2 mm resolution magnetic susceptibility values from both cores.

Two wood remnants and one cedar (*Cedrus atlantica* Manetti) needle from the recovered cores were processed at the Klaus Tschira ^{14}C laboratory in Mannheim (Table 2). Apart from these samples, systematic core screening every 2 cm at 125 μm and 250 μm failed to produce terrestrial plant macrofossils or sufficient quantities of charcoal for dating. As an alternative for diminishing a potential reservoir effect, dating of pollen concentrates (Fletcher et al., in press) is viable at Sidi Ali, as pollen concentrations are generally high (around 200,000 grains/cm^3). Following laboratory trials on Sidi Ali sediments, samples were prepared following the dense-media separation methodology of Vandergoes and Prior (2003) and submitted to NERC RCF East Kilbride, with AMS determinations made at either SUERC or, for the smallest samples, Keck C-Cycle Lab. Dating standards of both known age (IAEA-C5 wood: 11,780 ^{14}C years BP) and infinite age (anthracite and bituminous coal) were prepared in parallel, and indicated no detectable contamination with modern carbon during the preparation procedure. Additional determinations on pollen concentrate samples were completed at the Australian Nuclear Science and Technology Organisation.

All radiocarbon ages were calibrated using IntCal13 (Reimer et al., 2013). A Bayesian Poisson process deposition model (P_Sequence, Bronk Ramsey, 2008) was generated in OxCal v4.2 (Bronk Ramsey, 2009a) according to the available prior information (26 radiocarbon dates excluding bulk dates, 6 $^{210}Pb/^{137}Cs$ control points at decadal intervals, core-top age (2012 CE) and a boundary constraint on the basal age (14,000-10,000 cal BP)). The parameter k that

Table 2
Chronological data for Sidi Ali core. Calibration (2 sigma) of the conventional radiocarbon ages was performed using intcal13.14c. The Bayesian age model follows the approach of Fletcher et al. (in press).

ID code	Corrected depth [cm]	^{14}C Lab No.	Material	Age [*CE*, or ^{14}C yr BP]	Age [cal BP, 2σ]	Modelled age [cal BP, 2σ]	Modelled age [cal BP, μ]	$\delta^{13}C$ (‰)
Core top	0	–	–	*2012 CE*	–	−60 to −64	−62	–
Ali 11 23–24	0.5 (Ali 1)	SUERC-48007	Bulk sample	893 ± 35	911–734	n/a	n/a	−23.6
Ali 11 28–29	8.1 (Ali 1)	–	Pb^{210}/Cs^{137}	*2001 CE*	–	−49 to −53	−51	–
Ali 11 44–45	25.7 (Ali 1)	–	Pb^{210}/Cs^{137}	*1991 CE*	–	−39 to −43	−41	–
Ali 11 60–61	48.9 (Ali 1)	–	Pb^{210}/Cs^{137}	*1982 CE*	–	−30 to −34	−32	–
Ali 11 68–69	64.2 (Ali 1)	–	Pb^{210}/Cs^{137}	*1973 CE*	–	−21 to −25	−23	–
Ali 11 76–77	79.4 (Ali 1)	–	Pb^{210}/Cs^{137}	*1963 CE*	–	−11 to −15	−13	–
Ali 11 92–93	114.1 (Ali 1)	–	Pb^{210}/Cs^{137}	*1947 CE*	–	5–1	3	–
Ali 1 188–193	176.8	SUERC-60067	Pollen concentrate	630 ± 37	664–551	252–19	84	−21.9
Ali 11 130–131	177.8 (Ali 1)	MAMS 18507	Needle *Cedrus*	22 ± 18	237 to −6	250–40	87	N/A
Ali 1 197–200	182.6–185.5	OZT277	Pollen concentrate	1340 ± 40	1315–1181	575–41	224	−21.7
Ali 1 195–200 CC	197.5	UCIAMS-144601	Pollen concentrate	1920 ± 60	1992–1717	626–47	355	N/A
Ali 2 219–222	207.5–209.5	OZT278	Pollen concentrate	685 ± 45	693–554	654–52	419	−23.3
Ali 2 248–251	236.5–238.5	OZT279	Pollen concentrate	1245 ± 40	1274–1070	1109–232	653	−21.6
Ali 2 360–363	348.5–350.5	OZT280	Pollen concentrate	1915 ± 30	1934–1742	1551–818	1203	−21.8
Ali 2 388–390	377.0	SUERC-60068	Pollen concentrate	1956 ± 35	1988–1826	1601–956	1295	−23.8
Ali 2 391–396 CC	393.5	UCIAMS-144599	Pollen concentrate	1930 ± 30	1946–1820	1621–1005	1337	N/A
Ali 3 500–502	487.1–489.1	OZT281	Pollen concentrate	1755 ± 30	1736–1565	1705–1282	1529	−22.4
Ali 3 593–597 CC	595	SUERC-52698	Pollen concentrate	1929 ± 37	1987–1743	1930–1591	1779	N/A
Ali 4 610–612	604.3–606.2	OZT282	Pollen concentrate	2090 ± 25	2128–1994	2030–1624	1827	−21.9
Ali 4 707–709	696.8–698.7	OZT283	Pollen concentrate	2350 ± 45	2683–2187	2552–1908	2236	−22.3
Ali 4 796–800 CC	783	SUERC-49444	Pollen concentrate	3082 ± 37	3378–3184	3325–2470	2955	−24.6
Ali 5 904–905	892.5	MAMS 18377	Wood	3449 ± 18	2823–3640	3825–3640	3714	−29.0
Ali 5 993–994	978.7	MAMS 18378	Wood	3850 ± 20	4405–4157	4395–4156	4264	−19.7
Ali 5 993–994	978.7	SUERC-48010	Bulk sample	4224 ± 37	4857–4628	n/a	n/a	−24.3
Ali 5 997–1000 CC	998.5	SUERC-52694	Pollen concentrate	3990 ± 37	4568–4302	4462–4182	4325	−24.0
Ali 6 1109–1111	1100.7–1102.7	OZT284	Pollen concentrate	4520 ± 30	5305–5050	5265–4618	4962	−23.7
Ali 6 1195–1200 CC	1183.5	UCIAMS-133576	Pollen concentrate	5420 ± 20	6283–6198	6240–5274	5809	N/A
Ali 7 1309–1312	1301.1	SUERC-60069	Pollen concentrate	5937 ± 37	6877–6670	6834–6149	6559	−25.2
Ali 7 1397–1400 CC	1398.5	UCIAMS-133575	Pollen concentrate	7580 ± 35	8425–8345	8395–7349	7996	N/A
Ali 8 1509–1512	1497.0	SUERC-60070	Pollen concentrate	8462 ± 38	9531–9437	9500–8499	9123	−24.7
Ali 8 1597–1600 CC	1598.5	SUERC-49441	Pollen concentrate	9130 ± 41	10,408–10,221	10,359–9468	9978	−25.2
Ali 9 1709–1712	1695.0	SUERC-60073	Pollen concentrate	10,033 ± 42	11,751–11,333	11,387–10,134	10,777	−25.4
Ali 9 1795–1800 CC	1797.5	UCIAMS-133574	Pollen concentrate	10,045 ± 35	11,756–11,358	11,671–10,759	11,257	N/A
Ali 10 1964–1965	1953.3	SUERC-48011	Bulk sample	10,648 ± 43	12,703–12,555	n/a	n/a	−24.6
Ali 10 1954–1959 CC	1956.5	SUERC-52693	Pollen concentrate	10,343 ± 41	12,389–12,014	12,339–11,483	11,961	−24.8

determines the increment size and "flexibility" of the model was model-determined, from a starting value of 1 and allowing variation across two orders of magnitude in either direction (Bronk Ramsey and Lee, 2013). Outlier analysis was incorporated with outliers to be distributed according to an exponential distribution from −10 to 0 with a time constant of 1 and shifts scaled by up to 1000 yr (Bronk Ramsey, 2009b). Details of the pollen concentrate preparation and age model validation are presented in Fletcher et al. (in press).

3.12. Spectral analyses

In order to test for periodicities in the lake record, we used RedFit spectral analysis of the Sidi Ali carbonate data following the approach of Schulz and Mudelsee (2002). To further examine the evolution of periodic components and evaluate Holocene instationarities in the data, we used wavelet analysis following Torrence and Compo (1998). For both analyses, the carbonate data from both Scheibler analysis and scanning XRF are compared, in order to consider only results that are independent of the contrasting temporal resolution of the data series. Carbonate data were detrended by third-order polynomial prior to RedFit and wavelet analysis, effectively removing the main multi-millennial trends. Interpolation to the average intersample temporal difference (Scheibler measurements at 40 yr spacing; scanning XRF at 5 yr spacing) was undertaken for wavelet analysis only. Periodicities significant at the 95% level are reported.

4. Results

4.1. Bathymetric survey, lake-bottom characteristics and coring

The Sidi Ali bathymetry shows a doline-like basin with a maximum depth of 51 ms TWT (approx. 38 m) in the SW of the lake. A sill separates the main basin from a 31 ms TWT (approx. 23 m) deep sub-basin in the NE of the lake (Fig. 2a). In the shallower basin in the NE of the lake, the signal penetrates up to 50 ms TWT deep in the lake bottom, while maximum penetration depth amounts only 20 ms TWT in the deeper SW basin (Fig. 2b and c). The Sidi Ali seismic data indicate that mass transport deposits are not present at the drilling position. The drilling site is situated at the deepest location of the lake yielding a 19.63 m sequence from a single borehole (Fig. 2d, cores Ali 1 to 10). One additional short core (Ali 11, Fig. 2d) was recovered from a close-by position with a total length of 1.45 m.

4.2. Modern hydrochemical data from lake and surface waters

Based on the September 2012 survey, Lake Sidi Ali reveals an electric conductivity of 1.6 mS/cm at the lake surface, corresponding to a salinity of approx. 0.83 g/l. The water body displays alkaline conditions (pH 9.7, Fig. 4b), and features a high amount of Mg^{2+} (75 (eq)%). The content of Ca^{2+} is very low and reaches only 3 (eq)% (Fig. 3) although the catchment of the lake is rich in limestone. The low Ca^{2+} content points to a high precipitation of carbonates due to evaporation. HCO_3^- is the dominant anion at approx. 63 (eq)%. The SO_4^{2-} content reaches 30 (eq)%. The oligo- to mesotroph lake presents a Secchi depth of 2.1 m, a NO_3^- content of 0.34 mg/l, and an ortho-PO_4^{3-} content of 0.01 mg/l. Within the epilimnion $\delta^{18}O$ values are between 1.2 and 2.5‰, the δ^2H display values between 1.3 and 3.7‰ (Fig. 4a).

In the vicinity of the lake (Fig. 1b) marshland and spring waters show significantly lower $\delta^{18}O$ values between −8.8 and −5.9‰ and lower δ^2H values between −57.2 and −44.8‰ (Fig. 4a). The spring waters show balanced Ca and Mg contents indicating the dolomitic

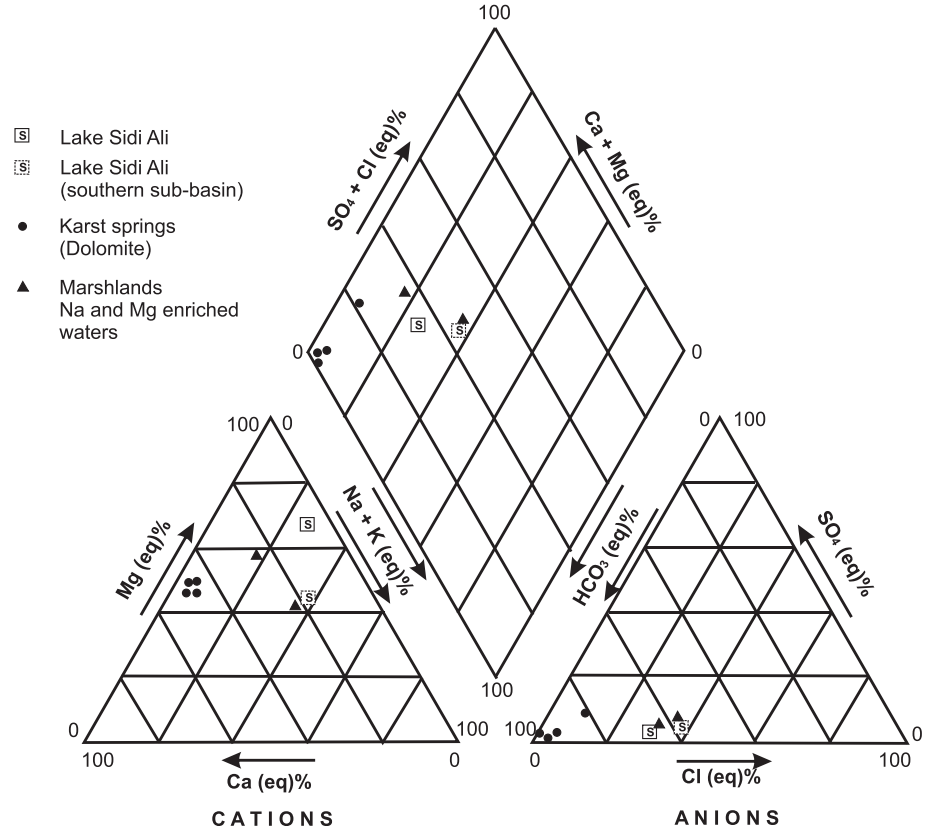

Fig. 3. Piper diagrams with modern hydrological data from Lake Sidi Ali and adjacent hydrological sites; for sampling positions see Fig. 1b.

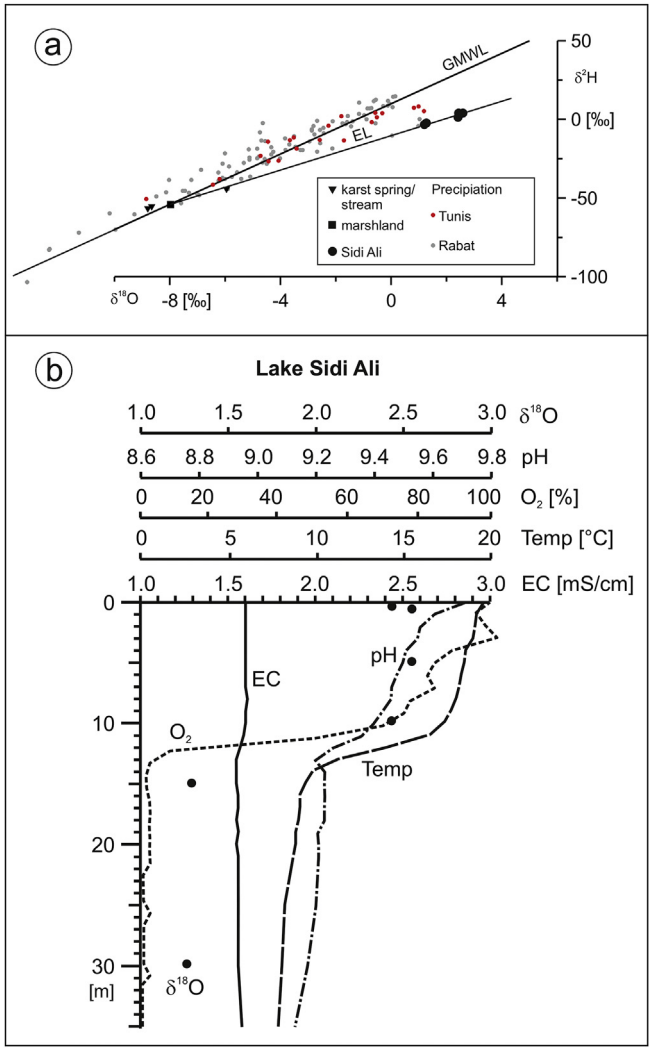

Fig. 4. Hydrological data from Lake Sidi Ali, showing: a) stable oxygen and hydrogen isotopes of modern hydrological samples (Lake Sidi Ali and springs [this study], Tunis precipitation events [Celle-Jeanton et al., 2001], Rabat precipitation events [Ouda et al., 2005]); for Sidi Ali sampling positions see Fig. 1b; b) hydrological water-depth profile from Sidi Ali conducted in September 2012.

origin of the seepage waters (Fig. 3). Low stable isotope values and the balanced Ca and Mg contents indicate that the stream and spring waters are not influenced by evaporation in contrast to the water in the lake. The Sidi Ali water-depth profile (N 33° 4′ 5.5″, W 4° 59′ 54″) reveals a water column of 35 m and displays a minimum temperature of 8 °C at the bottom of the lake. The hypolimnion is characterised by anaerobic conditions during summer (Fig. 4b).

4.3. TOC and carbonate contents, magnetic susceptibilities – stratigraphical units

All cores are characterised by horizontally bedded, faintly laminated, calcareous to lime silicic gyttja, with aquatic macrofossils including plant fragments (*Potamogeton*) and ostracods. The visual stratigraphy is very homogeneous (Table 1). The lower core section from Ali 8 to Ali 10 incorporates vivianite concretions of up to 5 mm in size.

Following the magnitudes and frequencies of TOC, carbonate contents (Fig. 8d and e) and values of magnetic susceptibility (Fig. 5a), the total core stratigraphy can be defined in terms of five major units and three subsequent subunits (Table 1). Blue coloured bars in Figs. 5 and 8 highlight higher-order variability. Peaks in carbonates typically coincide with peaks in magnetic susceptibilities and troughs in the TOC record.

4.4. XRF record

Selected silici-clastic XRF data are shown in Fig. 5. In Fig. 6 bivariate correlations between silici-clastic elements and volume magnetic susceptibility are presented. Strong positive correlations are also observed between the Ca values determined by core-scanning XRF and benchtop XRF Spectro ($R^2 = 0.75$), and core-scanning XRF and carbonate content by chemical digestion (Scheibler method) ($R^2 = 0.93$).

4.5. Diatom record, ostracod abundances and stable isotopes, Cedrus pollen record

The Sidi Ali diatom record reveals a dominance in most units of planktonic species of which *Cyclotella* sp. aff. *comensis* type 3 and type 1 are the most abundant (Fig. 7a and e). *Cyclotella* sp. aff. *ocellata* type 4 (Fig. 7d) and *Fragilaria* spp. (predominantly *Fragilaria brevistriata*) (Fig. 7f) represent species that are characteristic of intermediate depths. The most abundant epiphytic and/or littoral species in the Sidi Ali record are *Cocconeis placentula* (Fig. 7g), *Navicula* spp., and *Amphora* spp.

Fig. 8c displays total ostracod counts per sample. Figs. 8g and 9c show the C and O stable isotope records from ostracod shells. $\delta^{18}O$ and $\delta^{13}C$ show a significant anti-correlation ($r = -0.62$) for the total core.

We present the abundance of *Cedrus* pollen, reflecting the regional development of the cool tolerant and moisture-demanding conifer, *Cedrus atlantica* Manetti (Fig. 9b). Full details of the vegetation record will be explored elsewhere.

4.6. ^{210}Pb and ^{137}Cs radiometric dating and ^{14}C dating results

A ^{14}C age of 893 ± 35 cal BP on near surface bulk sediment from short core Ali 11 indicates a non-negligible component of old carbon in the lake system, as the results of the ^{210} Pb/^{137}Cs dating reflect a sub-recent age of deposition around 2004 (Table 2). This old carbon component may relate to a sub-recent reservoir effect of 950 years in the lake system. Table 2 shows the results from the reservoir effect diminishing ^{14}C pollen dating with the 2 sigma posterior ranges from the Bayesian model and incorporated outlier analysis. The modelled data show a robust sequence of Holocene ages with the core reflecting the last 12,000 years depositional history of Lake Sidi Ali (Fig. 10).

5. Discussion

5.1. Sidi Ali proxy parameters and derived mechanisms

5.1.1. Diatoms as lake-level and salinity proxies

Cyclotella sp. aff. *comensis* type 1 (Fig. 7e) is abundant in the uppermost part of our record reflecting current hydro-ecological conditions. This taxon is described by Barker et al. (1994) as planktonic *Cyclotella* aff. *comensis* Grunow. However, due to polymorphisms of the valves a clear assignment is difficult and *Cyclotella* aff. *comensis* Grunow is more typical for alpine and subalpine lakes (Krammer and Lange-Bertalot, 1991). Additionally, according to Gasse et al. (1995), the optimal ecological conditions for *Cyclotella comensis* correspond with 515 µS/cm, a lower conductivity than the current Lake Sidi Ali (Fig. 4b). *Cyclotella* sp. aff. *comensis* type 3 (Fig. A2d) is a planktonic species and most abundant in the

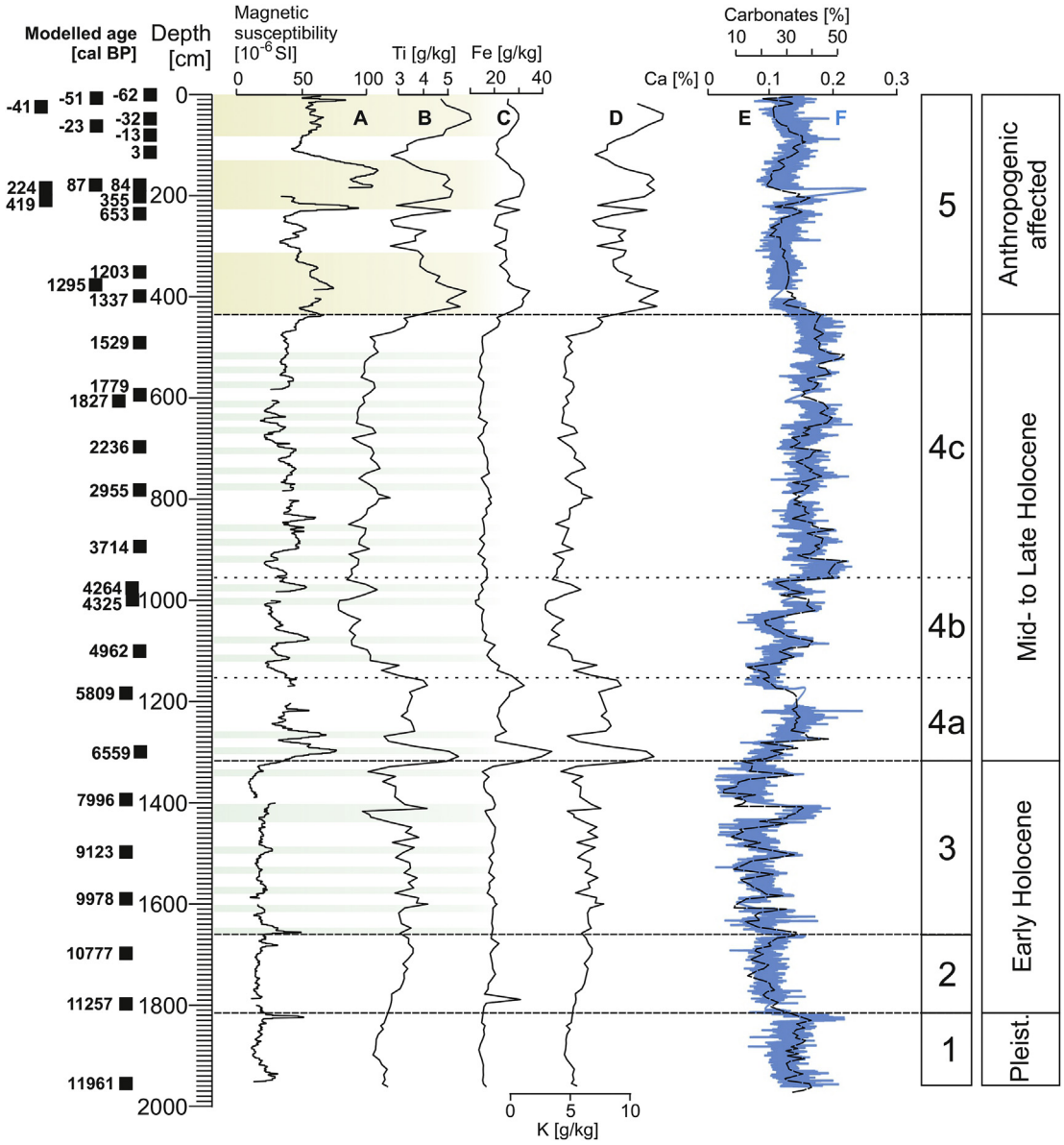

Fig. 5. Sidi Ali palaeomagnetic and silici-clastic proxies: a) volume magnetic susceptibility; b) XRF Ti content; c) XRF Fe content; d) XRF K content; e) carbonate content and f) calibrated Ca XRF scanning data. Blue bars indicate internal variability of magnetic susceptibility peaks, which are coeval with carbonate peaks (Fig. 8e) and TOC troughs (Fig. 8f). (For interpretation of the references to colour in this figure legend, the reader is referred to the web version of this article.)

core. This species is described by Barker et al. (1994) as *Cyclotella* sp. 1. Currently, *Cyclotella* sp. aff. *ocellata* type 4 (Fig. A2b) is not present at Sidi Ali but in other Middle Atlas lakes. The planktonic/littoral species is present in eutrophic lakes with lower salinity (<800 µS/cm, Flower et al., 1989; El Hamouti, 2003). Therefore, we interpret the abundance of this species as an indicator for a freshwater lake. *Cocconeïs placentula* (Fig. A2e) is a littoral epiphyte and typical for shallow lakes and dense aquatic plants (El Hamouti, 2003). The relative sum of saline (>3.2 mS/cm) diatom contents is used as an indicator for changes in salinity (Fig. 8b). High P/L ratios might indicate relatively elevated lake levels (Fig. 8a).

5.1.2. Lake internal productivity and lake level changes

High TOC represents enhanced lake-internal biomass production and/or anaerobic conditions at the lake bottom due to a high lake level (Meyers and Teranes, 2001). Hence, high TOC is predominantly the result of warm productivity seasons during phases of year-round high lake levels. Furthermore, a high lake level in a closed karstic basin suggests an elevated groundwater table. Reducing conditions driven by organic matter decomposition favour the incorporation of disulphides in the lake sediment, which is indicated by an enhanced S/Fe ratio (Fig. 8f) (Jones and Manning, 1994; Lucchini et al., 2003). The correlation between S/Fe and TOC is significantly positive (Fig. 6c, $R = 0.60$) for the total core. Using TOC as a proxy for the anaerobic preservation of organic matter, we postulate pyrite production with S_2^{2-} in solid state under anaerobic conditions.

The significant anti-correlation between TOC and carbonates for the total Sidi Ali core (Fig. 6a, $R = -0.49$) might be the result of the relative carbonate decrease due to increased algae productivity or the relative carbonate enrichment in times of low organic matter preservation. Generally, there seems to be evidence that the precipitation of carbonates at the lake bottom corresponds to aerobic hypolimnic conditions. This is shown by high ostracod abundances

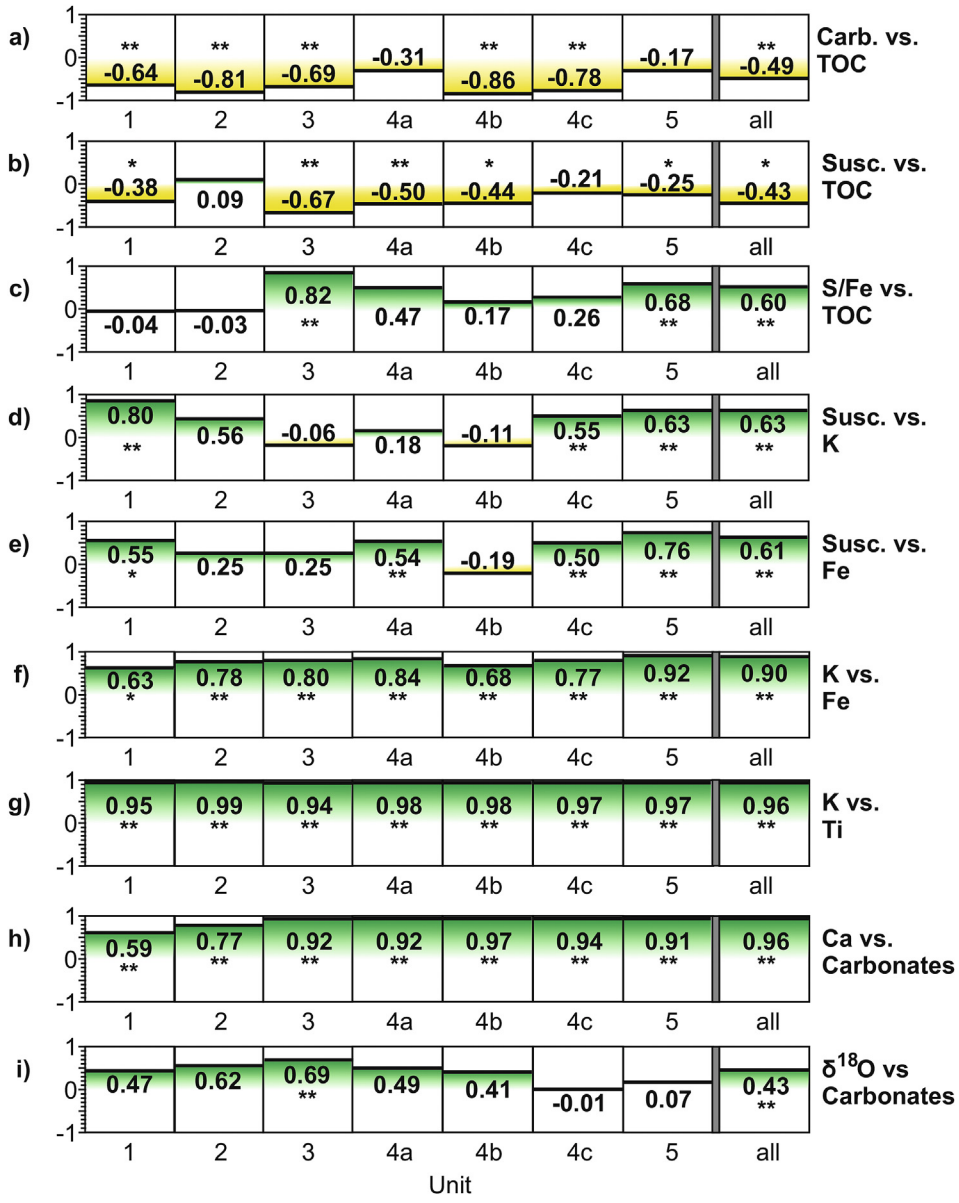

Fig. 6. Bivariate correlations between selected proxies within individual and all stratigraphical units. One asterisk indicates a level of significance (bilateral) of <0.05, two asterisk indicate a level of significance (bilateral) of <0.01.

(Fig. 8c) and enhanced magnetic susceptibilities (Fig. 11b) during phases of high carbonate deposition (Figs. 8d and 11e). Peaks in magnetic susceptibilities reflect aerobe conditions at the lake bottom and/or enhanced terrestrial influx. Simultaneous peaks in carbonates, peaks in magnetic susceptibilities and troughs in TOC might be therefore proxies for aerobic conditions at the lake bottom and/or low lake levels.

5.1.3. *Ostracod oxygen isotopes: seasonal shifts from winter to spring precipitation*

Sidi Ali water samples have $\delta^{18}O$ values between +1.21 and +2.57‰ vs. SMOW (Fig. 4). The $\delta^{18}O$ values of the epilimnion of Lake Sidi Ali are higher than those of bottom waters indicating the evaporative enrichment of surface waters during summer stratification. These values are comparable to the data of Benkaddour et al. (2005) that reveal a range from 0 to +5‰ vs. SMOW. We calculated the $\delta^{18}O$ values for carbonate formed in water of known oxygen isotope composition and temperature using the equation of Friedman and O'Neil (1977). We used measured (Fig. 4b) surface (18.5 °C) and bottom water temperatures (8.7 °C) to cover the range of possible $\delta^{18}O$ results. $\delta^{18}O$ values of modern spring and stream water samples are in the range from −9 to −6‰ vs. SMOW (Fig. 4a). These values are much lower than those of the lake as is to be expected for a closed basin setting.

As a result, carbonate formed in the spring and stream waters should have $\delta^{18}O$ values between −10 and −4‰ vs. PDB. This range covers the warm and cold temperatures given above. Carbonate formed in the modern Sidi Ali waters should have $\delta^{18}O$ values between +0.5 and +4‰ vs. PDB covering the warm and cold temperatures given above. This fits well with the youngest $\delta^{18}O$ value from Sidi Ali ostracod shells (Fig. 9c). For the total record the values range between +2 and +8‰ vs. PDB. These absolute values indicate that Sidi Ali was always a closed-basin lake during the total period covered by the core.

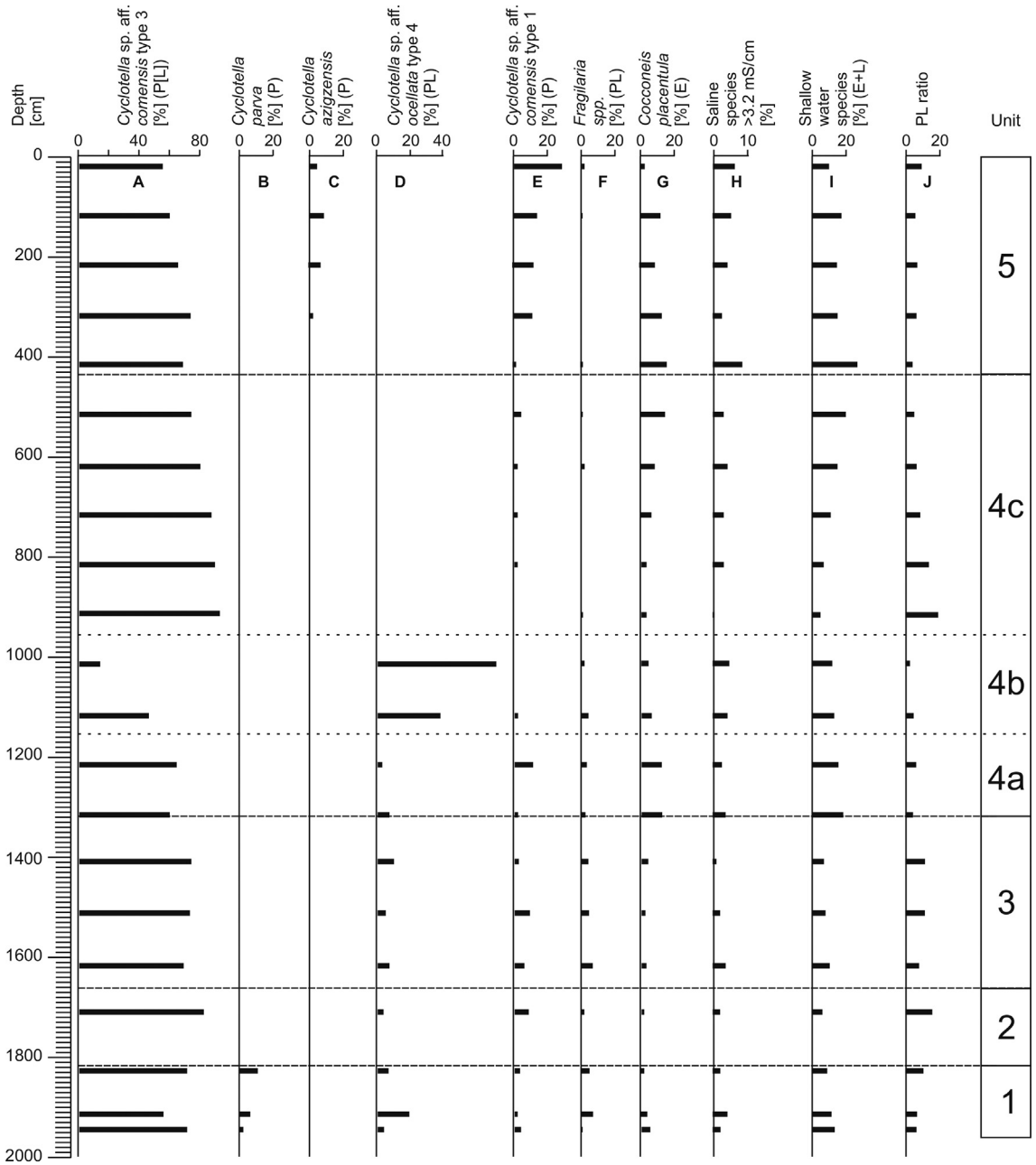

Fig. 7. First set of Sidi Ali diatom data: a) Planktonic *Cyclotella* sp. aff. *comensis* type 3, b) Planktonic *Cyclotella parva*, c) Planktonic *Cyclotella azigzensis*, d) Planktonic and littoral *Cyclotella* sp. aff. *ocellata* type 4, e) Planktonic *Cyclotella* sp. aff. *comensis* type 1, f) Planktonic and littoral *Fragilaria* spp. g) Epiphytic *Cocconeis placentula*, h) Epiphytic and littoral saline species, i) Epiphytic and littoral shallow water species, j) Planktonic/Littoral diatom ratio.

The Sidi Ali $\delta^{18}O$ record from ostracod shells shows significant sub-millennial-scale peaks in almost all units (Fig. 9c). There are two ways to interpret these $\delta^{18}O$ maxima:

I) $\delta^{18}O$ maxima result from drought conditions that reduce the local precipitation/evaporation ratio. This interpretation is the most straightforward in a semi-arid, closed lake setting (Roberts et al., 2008). However, some indications within the multi-proxy dataset are not coherent with this interpretation. In the lower part of the core (unit 3 and 4a) the $\delta^{18}O$ maxima correspond with minima in Sidi Ali macro-charcoal counts (Fig. 9a and c). As the Sidi Ali basin currently experiences a mean annual precipitation around 430 mm in a montane environment, the area seems generally too wet for a fuel limited fire regime (Carrión et al., 2003). Hence, the macro-charcoal minima reflect moisture during the growing season in contradiction to apparently drought derived peaks in the $\delta^{18}O$ signal. Additionally, the Sidi Ali macro-charcoal derived minima in fire activity conform to the newly generated *Cedrus* pollen record (Fig. 9b) that indicates moisture as well. A simple decrease of the P/E ratio with high $\delta^{18}O$ values would normally lead to a more xerophilous vegetation. This is not the case during the early Holocene at least, (e.g. units 3 and 4a), as the *Cedrus* pollen record suggests higher moisture availability in association with $\delta^{18}O$ maxima. However, this relationship changes over time towards a contrasting but

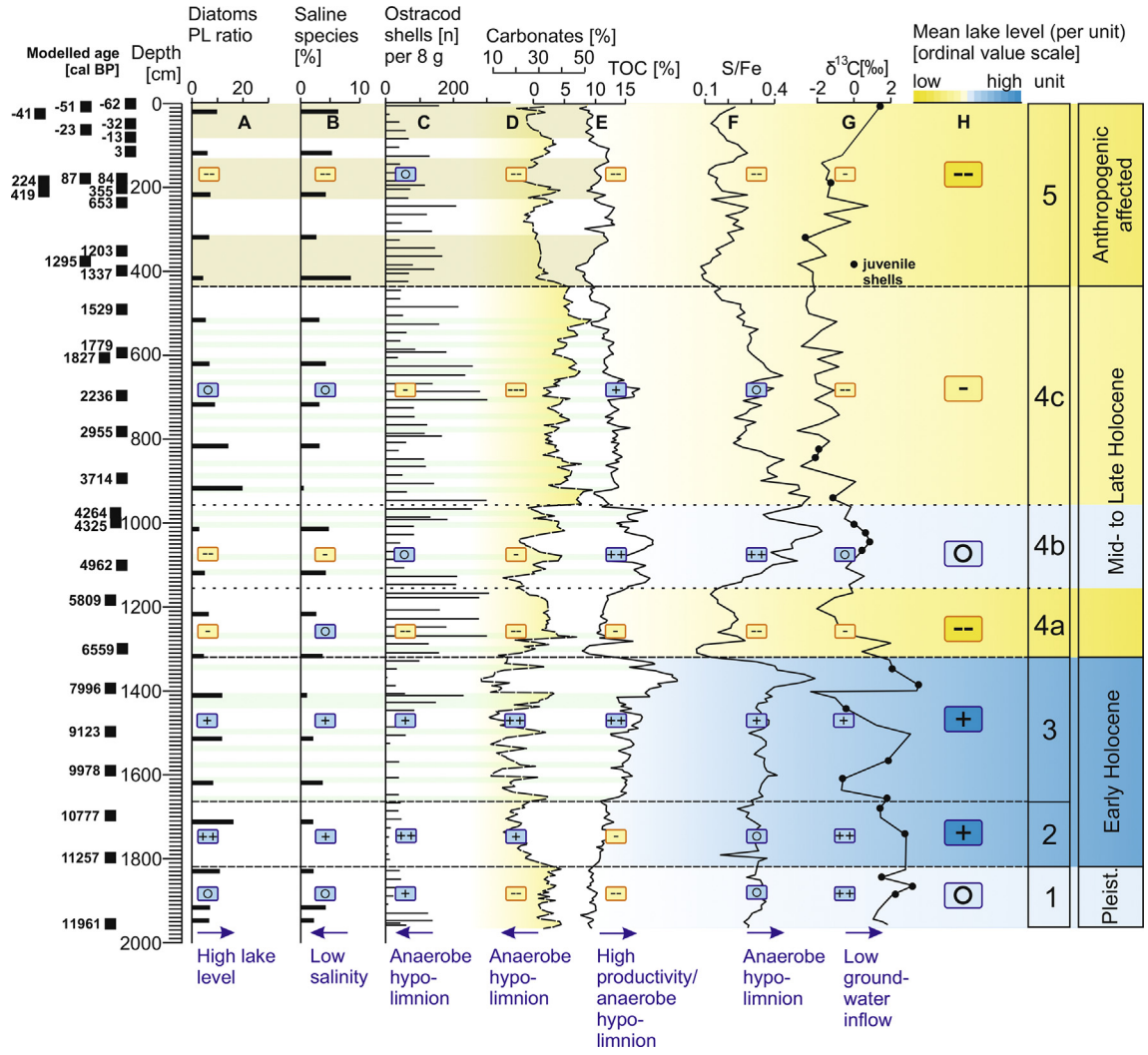

Fig. 8. Sidi Ali unit-scale lake level reconstruction: a) Planktonic/Littoral diatom ratio, b) saline diatom species (>3.2 mS/cm), c) total counts of ostracod shells per 8 g bulk sample, d) carbonate content, e) total organic carbon (TOC), f) S/Fe ratio, g) $\delta^{13}C$ from ostracod shell material, samples from partly juvenile ostracod shell material are signed with black dots, and h) ordinal-scale synthetic proxy (sum of "+" and "−" per sedimentological unit) for relative lake levels. Blue bars indicate internal variability of carbonate peaks and TOC troughs which are coeval with peaks in volume magnetic susceptibility (Fig. 6a). (For interpretation of the references to colour in this figure legend, the reader is referred to the web version of this article.)

typical pattern of a decreased P/E ratio with $\delta^{18}O$ peaks and troughs in the *Cedrus* curve (red arrows in units 4b, 4c, and 5; Fig. 9).

II) The second scenario is based on the assumption that high $\delta^{18}O$ values are the result of a specific origin and seasonality of the precipitation-bearing air masses. This view is supported by several lines of evidence. The current precipitation regime in the Middle Atlas is influenced by Western Mediterranean lows during spring and Atlantic winter cyclones (Knippertz et al., 2003). Precipitation from springtime Mediterranean lows reveals significantly higher $\delta^{18}O$ values than Atlantic winter rains due to its origin from the Mediterranean Sea (Moreno et al., 2014b). This can be also deduced from higher $\delta^{18}O$ values in modern precipitation from the Central Mediterranean (Fig. 4a) in comparison with lower values from the Moroccan Atlantic coast (Fig. 4a). Additionally, seasonally enhanced atmospheric spring temperatures will result in higher $\delta^{18}O$ values within spring precipitation (Roberts et al., 2008). Thus, a decrease in winter precipitation and a (relative) increase in spring precipitation could lead to higher $\delta^{18}O$ signals. This seems to be especially in evidence for Early to Mid-Holocene units 3 and 4a.

5.1.4. *Ostracod carbon isotopes: shifts in groundwater inflow*

The carbon isotopes of ostracod shells are influenced by diverse controlling factors: a) the ratio of groundwater inflow to surface runoff, with inflowing groundwater characterised by low $\delta^{13}C$ values and b) algal productivity, with higher productivity leading to the enrichment of the isotopically lighter ^{12}C, transport of lighter ^{12}C to the lake floor, availability there to ostracods, which form their shells there. Hence, the lowest $\delta^{13}C$ values may reflect high rates of groundwater inflow and/or higher algae productivity (Schwalb, 2002; Leng and Marshall, 2004).

Regarding the Sidi Ali $\delta^{13}C$ values, especially the units 4a to 5 reveal a positive trend with the TOC productivity proxy (Fig. 8e and g), which does not support the above mentioned coupling between low $\delta^{13}C$ values and high productivity. Hence, low $\delta^{13}C$ values seem to reflect more the impact of inflowing groundwater. We should expect a larger relative contribution of groundwater during dry

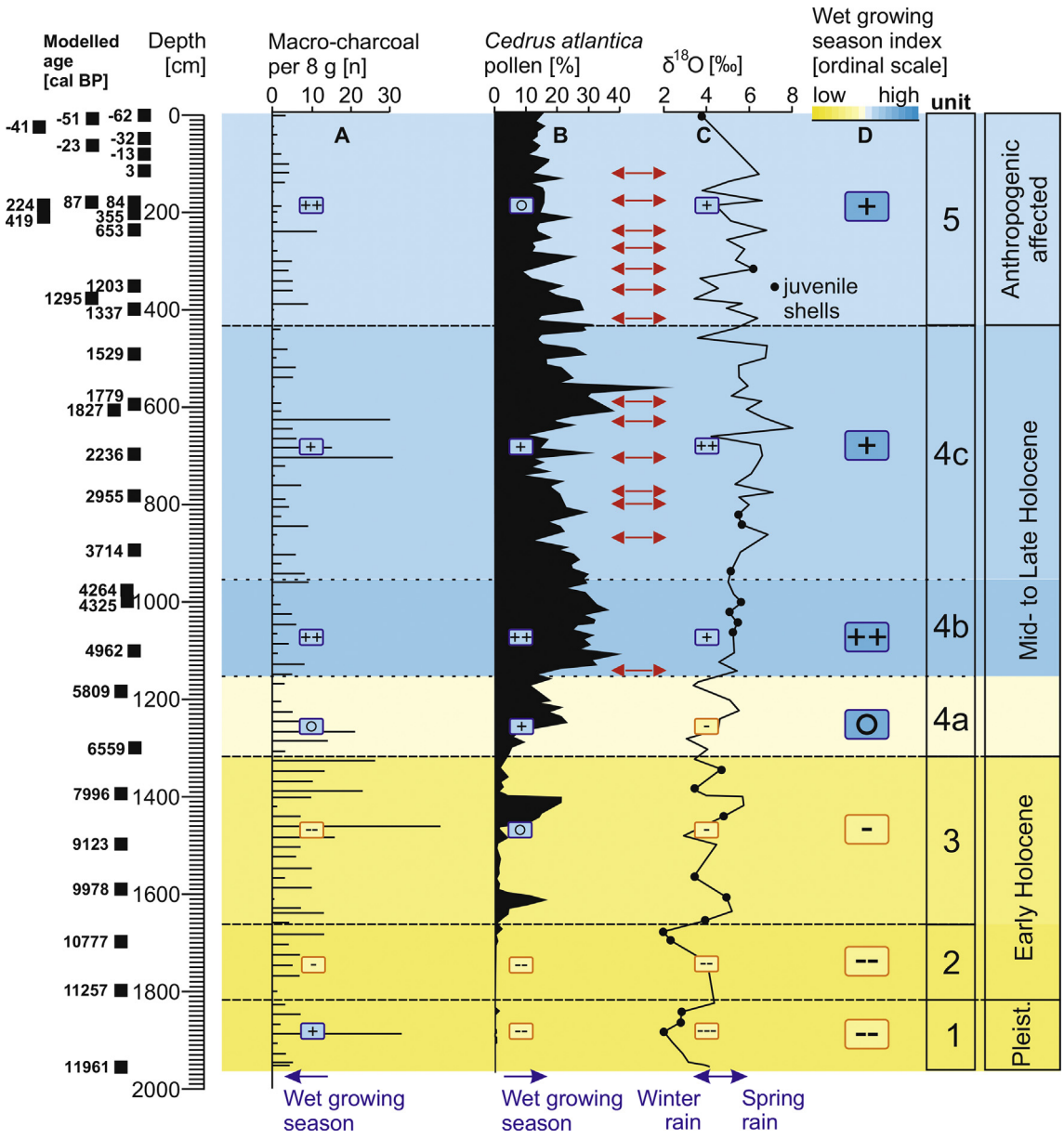

Fig. 9. Sidi Ali unit-scale humidity reconstruction for the growing season: a) macro-charcoal counts, b) *Cedrus atlantica* Manetti pollen record, c) $\delta^{18}O$ record from *Fabae-formiscandona* sp. and *Candona* sp., and d) ordinal-scale synthetic proxy (sum of "+" and "−" per sedimentological unit) for humidity during the growing season. Red arrows indicate centennial-scale *Cedrus atlantica* minima and peaks in $\delta^{18}O$ during the Mid- and Late Holocene. (For interpretation of the references to colour in this figure legend, the reader is referred to the web version of this article.)

phases of low lake level, and correspondingly a less strong influence of groundwater during wetter phases. According to this, unit 4a, the upper part of 4c and the onset of unit 5 indicate lower lake levels with high rates of groundwater inflow (Fig. 8g). Unit 3 shows high sub-millennial scale alternations in the $\delta^{13}C$ signal, which might reflect high amplitudes in lake level changes. Overall, the significant anti-correlation between $\delta^{18}O$ and $\delta^{13}C$ ($r = -0.62$) for the total core is not common for closed basin lakes (Talbot, 1990).

5.2. Long-term hydro-climatic history at Lake Sidi Ali

5.2.1. Younger Dryas (unit 1) from 12.0 to 11.4 cal ka BP

Chronologically, unit 1 comprises the last centuries of the Younger Dryas and onset of the Holocene (Rach et al., 2014). Several features suggest a cold climate with a relatively shallow lake environment, including low TOC contents (Fig. 8e) and a low P/L ratio (Fig. 8a). *Mastogloïa smithii* (Fig. A2g) and other saline species (Fig. 7h) are relatively abundant and might indicate enhanced saline conditions. To date, the climate during the Younger Dryas in North Africa and the Western Mediterranean is still incompletely known. In a broader sub-regional context there is evidence for lower temperatures and aridity during the Younger Dryas as indicated by low Alboran Sea surface temperatures (Cacho et al., 2001) and peaks in semi-desert pollen assemblages from Alboran Sea marine cores (Fletcher and Sánchez Goñi, 2008). However, a speleothem record from the Iberian Peninsula indicates increasing humidity during the second half of the Younger Dryas (Bartolomé et al., 2015), which might be an explanation for the assumed Younger Dryas glacier advances in the High Atlas (Hughes et al., 2011).

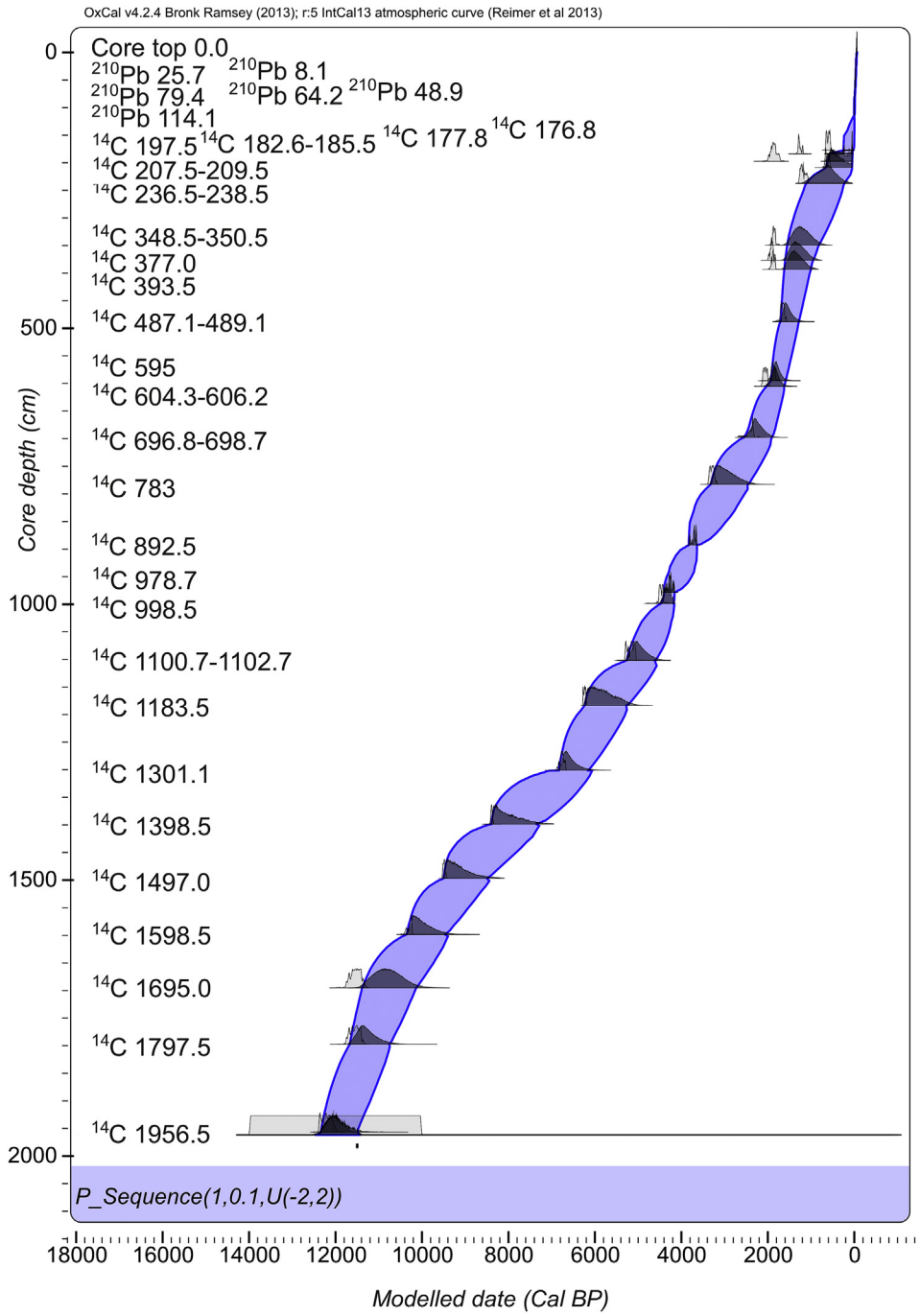

Fig. 10. Bayesian age model of the Lake Sidi Ali core stratigraphy following the approach of Fletcher et al. (in press).

5.2.2. Early Holocene (unit 2) from 11.4 to 10.5 cal ka BP

Unit 2 represents the first half of the Early Holocene (cf. Preboreal) and shows an increase in lake level and productivity due to rising TOC values (Fig. 8e). The diatom record points to an enhanced lake level due to a relatively high P/L ratio (Fig. 8a). The $\delta^{13}C$ values are high (Fig. 8g), indicating probably a high lake level with a high contribution from precipitation as opposed to groundwater inflow. These proxies point to a warm and relatively wet climate. Low numbers of ostracod shells (Fig. 8c) indicating an anaerobic lake bottom also support this interpretation. Low $\delta^{18}O$ values (Fig. 9c) might point to the dominance of Atlantic-derived winter rains.

5.2.3. Early to Mid-Holocene (unit 3) from 10.5 to 6.7 cal ka BP

Unit 3 is characterised by a strong increase in TOC with high variability. The TOC curve reaches its absolute maximum around 7.5 cal ka BP (Fig. 11c) indicating a high lake level and high productivity (Meyers and Teranes, 2001). This is supported by high S/Fe ratios (Fig. 8f), indicating an anaerobic lake bottom. The S/Fe ratio is positively correlated with TOC (Fig. 6c, $R = 0.82$). The $\delta^{13}C$ values reveal strong variability (Fig. 8g) indicating high amplitudes of lake level variability and shifts in relative precipitation-groundwater contribution.

5.2.4. Mid-Holocene (unit 4a) from 6.7 to 5.4 cal ka BP

The onset of unit 4a represents the most striking change of the entire core record. The TOC curve and S/Fe ratios display a noticeable and long-term minimum (Fig. 8e and f) reflecting low lake internal productivity and/or aerobic conditions at the lake-floor. These data correspond with carbonate maxima (Fig. 8d), high numbers of shallow water reflecting ostracod shells (Fig. 8c) and shallow water diatom species (Fig. 8a). Here, maximum abundances of epiphytic *Cocconeïs placentula* indicate very low lake levels with swampy environments and aquatic plants (Fig. 7g). Strongly increased magnetic susceptibilities (Fig. 5a) are positively correlated with Fe (Fig. 6e, R = 0.54) revealing an enrichment of terrestrial material.

5.2.5. Mid-Holocene (unit 4b) from 5.4 to 4.1 cal ka BP

Unit 4b features centennial-scale peaks in magnetic susceptibilities and carbonate contents and troughs in TOC (Figs. 5a and 8d and e). The high anti-correlation between carbonates and TOC (Fig. 6a, R = −0.86) points to the dominance of lake internal factors on the deposition process at the lake bottom. Unit 4b reveals a very low P/L ratio (Fig. 8a) and is characterised by a dominance of *Cyclotella* sp. aff. *ocellata* type 4 (Fig. 7d) that might indicate a shallow lake (Barker et al., 1994) but also an increasing inflow of freshwater (El Hamouti, 2003). The latter is supported by rising S/Fe (Fig. 8f) and TOC contents (Fig. 8e). This reflects a return to high lake productivity with an anaerobic hypolimnion. Decreased numbers of ostracod shells also suggest a higher lake level (Fig. 8c). In unit 4b, the number of macro-charcoal counts is low (Fig. 9a) and the *Cedrus* record (Fig. 9b) shows a maximum which suggests more humidity during the growing season.

5.2.6. Late Holocene (unit 4c) from 4.1 to 1.4 cal ka BP

Within the lower section of unit 4c the maximum of the diatom P/L ratio (Fig. 8a) points to a high lake level. The dominance of planktonic *Cyclotella* sp. aff. *comensis* type 3 (Fig. 7a) coincides with the disappearance of *Cyclotella* sp. aff. *ocellata* type 4. Towards the transition to unit 5 the decreasing amounts of *Cyclotella* sp. aff. *comensis* type 3 as well as a decreasing P/L ratio and increasing contents of epiphytic *Cocconeïs placentula* (Fig. 7g) indicate a gradual lake level decrease. We interpret a decreasing S/Fe trend (Fig. 8f) and increasing numbers of ostracods (Fig. 8c) towards the upper part of unit 4c as an increase in oxygen availability. To sum up, the Late Holocene shows in the beginning a relative high lake level but with a clear decreasing trend towards the upper section.

5.2.7. Unit 5 from 1.4 to −0.062 cal ka BP – human impact

Magnetic susceptibilities show an absolute maximum and are significantly positive correlated with K (Fig. 6d, R = 0.63) and Fe (Fig. 6e, R = 0.76). Pale brown bars in unit 5 (Figs. 5 and 8) show parallel fluctuations in magnetic susceptibility, Fe, Ti, and K versus the TOC record. These fluctuations seem to reflect an inorganic signal from soil erosion in the catchment that lowers TOC. The core stratigraphy shows rhythmic sediment layering (Table 1). Therefore, we discard potential evidence for a slump or turbidity current and assume increased soil erosion with continuous terrestrial influx into the lake. This might reflect a more open vegetation cover due to grazing, reflecting increasing human impact (Linstädter and Baumann, 2013; Cheddadi et al., 2015).

All diatom samples from the uppermost unit 5 indicate a maximum of planktonic *Cyclotella* sp. aff. *comensis* type 1 (Fig. 7e). However, noticeable amounts of *Cocconeïs placentula* (Fig. 7g) and a generally low P/L ratio (Fig. 8a) reflect relatively low lake levels. The S/Fe ratio is low (Fig. 8f) reflecting aerobic conditions at the lake floor.

5.3. Forcing of Western Mediterranean hydro-climatic variability and seasonality

5.3.1. Orbital-scale shift in Holocene hydro-climatic seasonality

The overall enrichment trend of the $\delta^{18}O$ signal (Fig. 9c) from the Younger Dryas to the onset of the Late Holocene might be the result of either long-term evaporative enrichment of ^{18}O or a long-term seasonality change from winter to spring precipitation with relatively more Mediterranean Basin-derived spring precipitation during the Late Holocene. The associated increase in plant available moisture might underlie the Mid-Holocene increase in *Cedrus* pollen at Sidi Ali (Fig. 9b).

For the Early Holocene Lamb and van der Kaars (1995) and Tabel et al. (2016) reveal a dominance of evergreen *Quercus* in the Middle Atlas reflecting a warm and relatively dry climate. This corresponds also with the northernmost position (29 °N) of the African monsoon (Meyer et al., 2013) and with a high summer insolation at that time (Berger, 1978, Fig. 11d). A summer cooling trend towards the Late Holocene will have reduced bioclimatic heat stress in the Middle Atlas. Hence, we assume that the increased Mid- to Late Holocene available moisture at Sidi Ali (Fig. 9d) and at other sites in the Middle Atlas (Lamb et al., 1995; Nourelbait et al., 2014; Tabel et al., 2016) might be also the result of lower summer temperatures and lower evaporation.

Other Middle Atlas palaeohydrological studies also detect the surprising mismatch between plant available moisture and the local hydrological water balance. Whereas the pollen data indicate humidity, the lake level remains low. Lamb et al. (1995) and Lamb and van der Kaars (1995) detect maxima in plant available moisture that coincide with low lake levels at Lake Tigalmamine. The authors assumed a probable lowering in winter precipitation that did not affect humidity during the growing season, but which will have significantly reduced groundwater recharge. Equally, Lamb et al. (1999) interpreted the Mid- to Late Holocene *Cedrus* pollen rise within the Sidi Ali sub-basin record as an indicator for increasing available moisture. In both that work and the present study, the *Cedrus* record does not really fit with changes in lake level. Hence, the authors do not infer more precipitation from *Cedrus* pollen rises, but rather more available moisture that may be the result of lower summer temperatures. Regarding our own data, the *Cedrus* pollen record (Fig. 9b) indicate more humidity during the Late Holocene, whereas the majority of our lake level proxies point to a general trend in Late Holocene lake level lowering (Fig. 8). Hence, the new Sidi Ali record also points to an overall transition from Early Holocene high winter precipitation towards Late Holocene low winter precipitation with more available moisture during cool summers. The reduction in winter precipitation over the course of the Holocene is consistent with insolation changes over the half precession cycle (minimum to maximum precession) as recently modelled by Bosmans et al. (2015). In this study, reduction in winter precipitation and relative increase in spring-autumn precipitation over the Holocene is linked to both the reduced passage of Atlantic storms over the western Mediterranean and changes in regional convection activity.

In contrast to the Middle Atlas, the Holocene hydro-climatic situation in the thermo-Mediterranean lowlands differs: a warm Early Holocene with rather dry climatic conditions in the Middle Atlas corresponds with a maximum in temperate and Mediterranean forest occupation in the lowlands (Fig. 11m). Regarding the Mid- to Late Holocene, the lowland records document an increase in aridity (Fletcher et al., 2010; Vannière et al., 2011; Magny et al., 2012) whereas the widespread *Cedrus* occupation in the Middle Atlas (Fig. 9b, Lamb et al., 1995; Tabel et al., 2016) suggests more moisture with a general cooling trend. This phenomenon can be linked to a sensible view that lowland vegetation is more sensitive

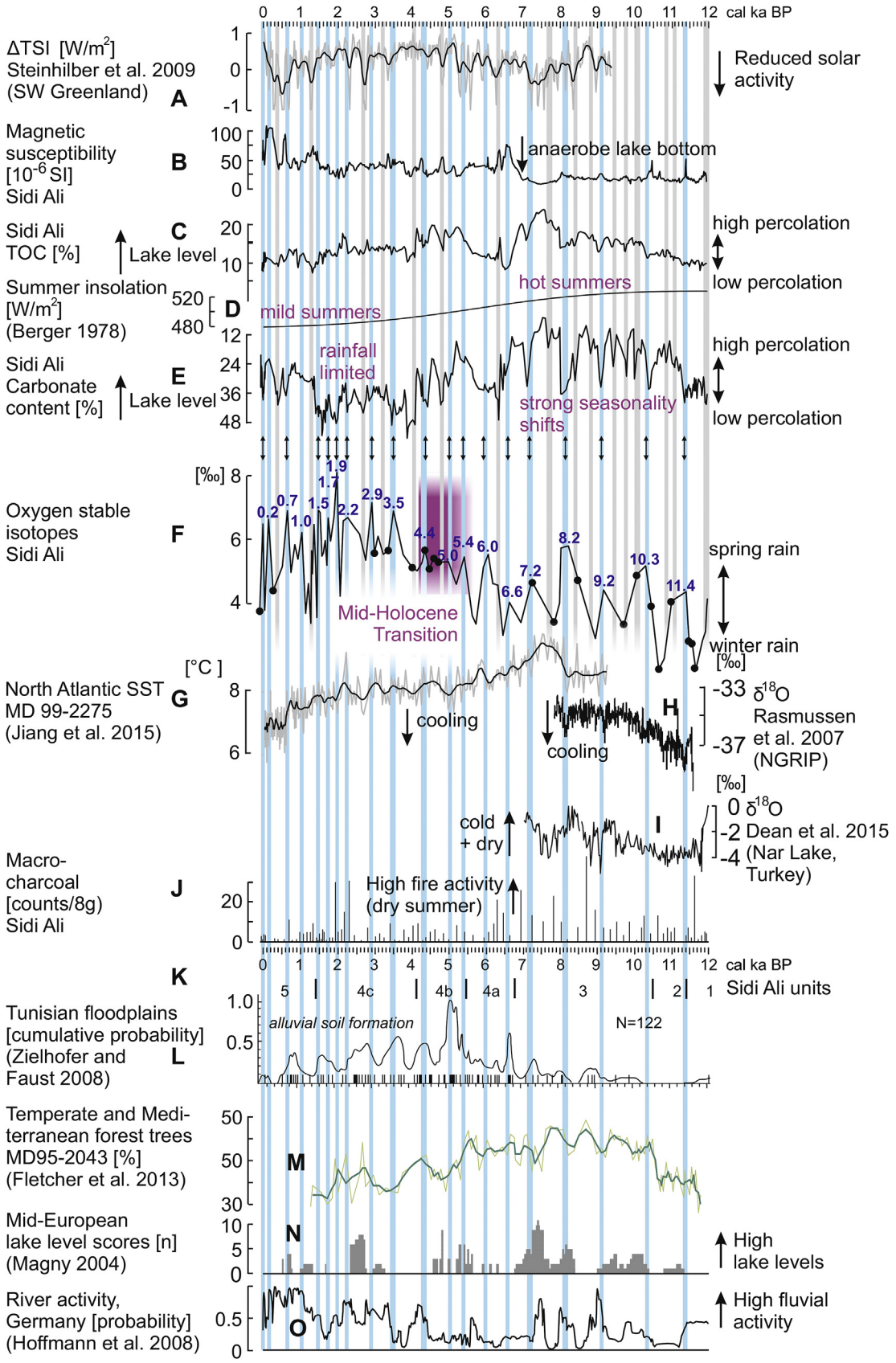

Fig. 11. Sidi Ali climatic proxy parameters in comparison with North Atlantic, Mediterranean and Central European climatic records: a) Δ Total solar irradiance [W/m^2] (Steinhilber et al., 2009); b) Sidi Ali volume magnetic susceptibility [10^{-6} SI units]; c) Sidi Ali TOC record (maxima represent high lake levels and/or high lake internal productivity) [%]; d) summer insolation curve (65°N, June, Berger, 1978) [W/m^2]; e) Sidi Ali carbonate record [%] (maxima represent low lake levels and/or low lake internal productivity); f) Sidi Ali ostracod derived $\delta^{18}O$ record [‰], the blue numbers [cal ka BP] indicate *Western Mediterranean winter rain minima* ($\delta^{18}O$ maxima); g) Sub-polar North Atlantic sea surface

to hydrological stress and upland vegetation to thermic stress. Furthermore, while lowland thermo-Mediterranean ecosystems may be sensitive to reduced winter precipitation related to the Mid- to Late Holocene aridification trend, montane vegetation may be less affected by reduced winter precipitation due to limited bioavailability of snow, but favoured by reduced summer temperatures and lower growing-season moisture stress.

5.3.2. Sub-millennial-scale hydro-climatic variability during the Early and Mid-Holocene

Especially during the Early and Mid-Holocene, the Sidi Ali proxy data show a significant sub-millennial-scale hydro-climatic variability. Phases of low lake level can be deduced from high carbonate values (Fig. 8d) that coincide with decreased TOC preservation potential at the lake floor (Fig. 8e) and enhanced abundances of ostracod shells (Fig. 8c). These sub-millennial-scale phases of low lake level correspond with increased $\delta^{18}O$ values (Fig. 9c: e.g. at depths of 1470, 1390 and 1330 cm). In contrast to these indications of low lake level status, charcoal minima point to more humidity and corresponding *Cedrus* pollen peaks (Fig. 9b) support this assumption. Minima in charcoal and peaks in *Cedrus* pollen are associated with high $\delta^{18}O$ values. As such, the orbital $\delta^{18}O$ trend from the Early to Late Holocene is detectable in the sub-millennial timescale as well, and the same overall interpretation may apply. Mediterranean-derived humidity (Moreno et al., 2014b) and warmer spring precipitation reveal higher $\delta^{18}O$ values (+0.45 per mil/°C, Roberts et al., 2008) than Atlantic winter rain. Therefore, we postulate that changing air mass origins coupled with changes in hydro-climatic seasonality control the $\delta^{18}O$ signal at sub-millennial timescales. During the Early and Mid-Holocene, high $\delta^{18}O$ values are the result of reduced winter precipitation and relatively enhanced spring precipitation. Additionally, increased plant available moisture during spring might be the result of cooling and reduced evaporation. Our multi-proxy approach suggests that sub-millennial-scale $\delta^{18}O$ maxima centred at 11.4, 10.3, 9.2, 8.2, 7.2, 6.6, 6.0, 5.4, and 5.0 cal ka BP (Fig. 11f) represent decreases in winter rain and relatively enhanced spring precipitation during overall annual cooling.

In the Western Mediterranean context, reduced winter rain and enhanced available moisture in the Middle Atlas appear to coincide with drier conditions in the Mediterranean lowlands also at sub-millennial timescales, as suggested by temperate and Mediterranean forest pollen declines in marine core MD95-2043 around 10.1, 9.2, 8.3, 7.4, and 5.9 cal ka BP (Fig. 11m). Enhanced $\delta^{18}O$ values, respectively winter rain minima, also noticeably correspond with Holocene cooling events in the sub-polar North Atlantic (Fig. 11g, Jiang et al., 2015) and show a similar frequency pattern as the North Atlantic ice-drifted debris record (Bond et al., 2001). These Early to Mid-Holocene Atlantic cooling events are also visible in Greenland ice cores (Fig. 11h, Rasmussen et al., 2007) and in terrestrial records across North America (Hou et al., 2012), Europe (Lang et al., 2010) and the Mediterranean Basin (Fig. 11i). Major Early Holocene Atlantic cooling events are probably driven by meltwater dynamics from the decaying ice-sheets around the North Atlantic (Heiri et al., 2004; Fletcher et al., 2013). We conclude overall annual cooling during these events at Sidi Ali but also in the large-scale North Atlantic realm. Atlantic cooling events corresponded with noticeable decreases in Western Mediterranean winter precipitation (Fig. 11f) and influenced larger-scale hydro-climate in Europe and the Eastern Mediterranean Basin, too. An increasing number of palaeo-hydrological studies indicate that in the Eastern Mediterranean region Early to Mid-Holocene Atlantic cooling events coincide with dry phases, too (Dean et al., 2015; Lespez et al., 2016). The overall timing and pattern of Sidi Ali-derived cooling events and Western Mediterranean winter rain minima is also shown in fluvial dynamics in the Central Mediterranean (Fig. 11l, Zielhofer and Faust, 2008) with phases of reduced flooding and alluvial soil formation during Early to Mid-Holocene winter rain minima. Moreover, high lake levels (Fig. 11n, Magny et al., 2004) and flooding in Central Europe (Fig. 11o, Hoffmann et al., 2008) might coincide with Western Mediterranean Winter rain minima during the Early to Mid-Holocene. Therefore, we suggest a northward shift of westerly winter storm tracks during sub-millennial Atlantic coolings, consistent with intensified zonal flow driven by enhanced temperature gradients in the North Atlantic during high-latitude cooling episodes (Fletcher et al., 2010).

5.3.3. Solar imprints and the mid-Holocene transition

In addition to the strong millennial variability expressed in the hydrological proxies, especially during the early Holocene, an additional, centennial-scale dynamic is evident at Sidi Ali. Maxima in magnetic susceptibilities (Fig. 11b) and carbonates (Fig. 11e) correspond with minima in TOC (Fig. 11c), as shown by grey bars (Fig. 11). There are significant anti-correlations between carbonates and TOC (Fig. 6a, $R = -0.49$) and between magnetic susceptibilities and TOC (Fig. 6b, $R = -0.43$). These dynamics reflect changes in the oxic/anoxic status of the lake sediment surface and allow the identification of centennial-scale lake productivity and/or lake level minima probably due to solar forcing (Fig. 11a, Steinhilber et al., 2009). The RedFit spectral and wavelet analyses of the discrete and XRF scanning (5 yr mean) calcite records (Fig. 12) suggest solar imprints: the results are very similar for both records with strong millennial and centennial variability. The RedFit spectral analysis suggests a ~2410 yr cycle (Fig. 12e) that might correspond with the Hallstatt cycle (Steinhilber et al., 2012), although the wavelet analysis of the higher resolution Ca XRF scanning data suggests there might be two separate low frequency cycles around 3000 yr and 1800 yr (Fig. 12d). Hallstatt-type solar cycles might be a driver for low frequency bimillennial-scale hydro-climatic periodicity in the North Atlantic realm (Ojala et al., 2015). The ~1000 yr Eddy cycle (Steinhilber et al., 2012) in the Early Holocene is clearly detectable (Fig. 12c and d). There is also strong variability around 340 yr period (Fig. 12), which is recognised in solar data. Steinhilber et al. (2012) report an "unnamed cycle at approximately 350 yr" in the power spectrum of solar activity that is detectable in numerous other palaeoclimatic records all over the world (Soon et al., 2014), but especially well-known from palaeo-monsoon records (Duan et al., 2014). The authors suggest that the solar signal may result from interactions with the ocean component of the Earth system such as variation in the North Atlantic thermohaline circulation. The ~200 yr band of the Sidi Ali carbonate record (Fig. 12e) is close to solar variability as these bands may reflect periodic signals of the de Vries (~210 yr) solar cycle (Steinhilber et al., 2012) that are known from numerous palaeoclimatic records all over the world

temperatures from core MD 99-2275 (Jiang et al., 2015); h) Early Holocene Greenland $\delta^{18}O$ record (NGRIP, Rasmussen et al., 2007); i) Early Holocene Turkey (Nar Lake) $\delta^{18}O$ record (Dean et al., 2015); j) Sidi Ali marco-charcoal counts [counts/8 g]; k) Sidi Ali units (according to Table 1); l) ^{14}C cumulative probability plots of Tunisian alluvial soil formation phases (Zielhofer and Faust, 2008); m) Temperate and Mediterranean forest trees [%] (MD95-2043 core, Fletcher et al., 2013); n) Central European high lake level scores [N] (Magny, 2004); o) Central European river activity (Hoffmann et al., 2008). Grey bars represent centennial-scale Sidi Ali carbonate maxima, magnetic susceptibility maxima, and TOC minima indicating decreases in lake level and/or decreases in productivity due to external forcing). Blue bars show the same pattern but corresponds additionally with Sidi Ali $\delta^{18}O$ maxima (winter rain minima) and represent lake level decreases due to *Western Mediterranean winter rain minima*. (For interpretation of the references to colour in this figure legend, the reader is referred to the web version of this article.)

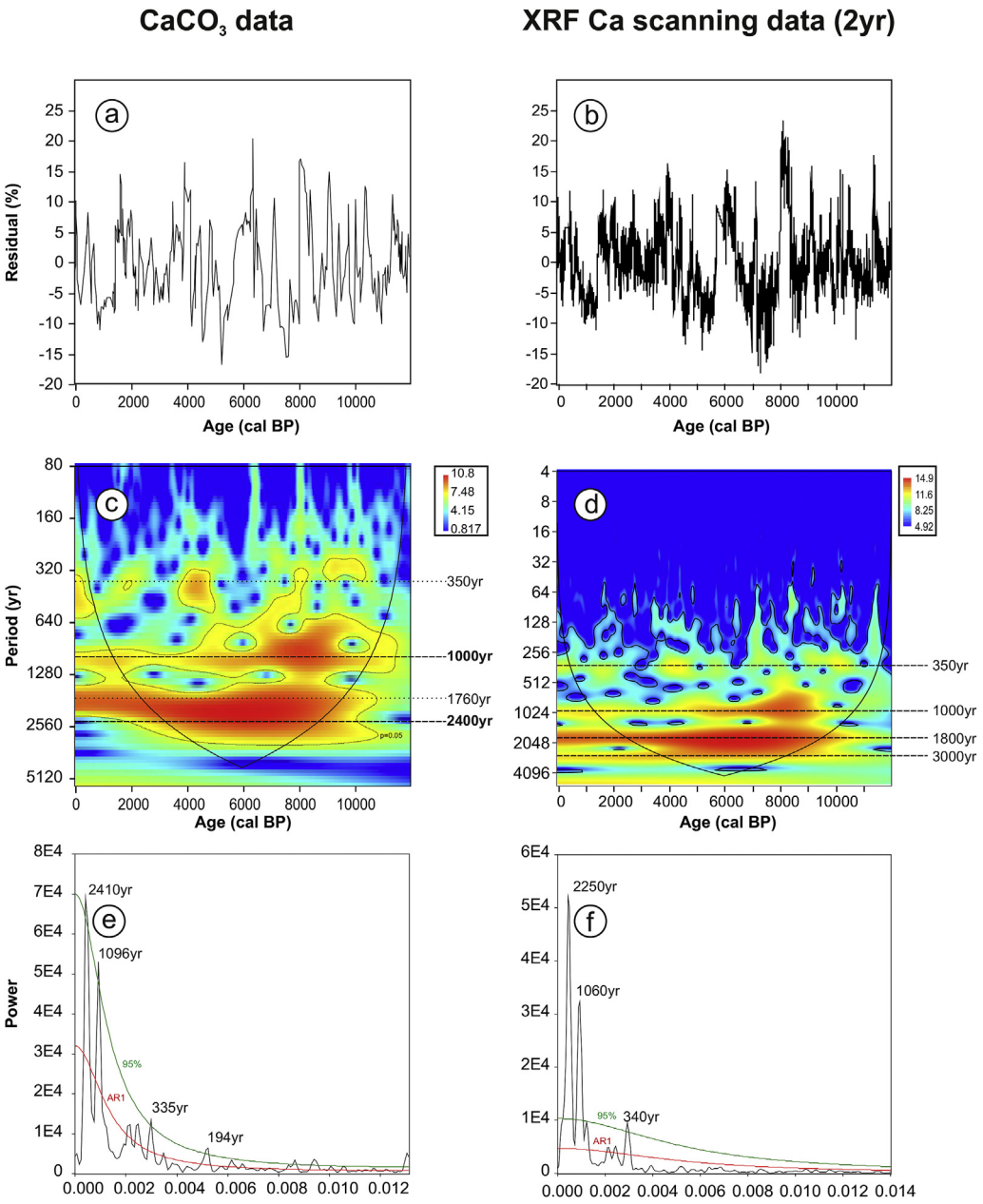

Fig. 12. RedFit spectral and wavelet analyses of carbonate and Ca XRF scanning data: a) and b) detrended values [3rd order polynomial], c) and d) wavelet diagrams showing cone of influence and p = 0.05 significance level, e) and f) RedFit spectral power diagram, showing Ar1 model (red) and 95% confidence limit (green). (For interpretation of the references to colour in this figure legend, the reader is referred to the web version of this article.)

(Duan et al., 2014; Ojala et al., 2015).

The wavelet analysis of the carbonate record clearly shows the strong ~1000 yr signal during the Early and Mid-Holocene (Fig. 12c and d) that is reduced in the Late Holocene. These Carbonate maxima (Fig. 11e) correspond not only with North Atlantic cooling cycles (Fig. 11g and h) but also coincide significantly with ~1000 yr cyclic winter rain minima (peaks in $\delta^{18}O$, Figs. 6i and 11f).

Although the Sidi Ali $\delta^{18}O$ record reveals a lower resolution (~130 yr) than the carbonate record (~40 yr), it seems that the $\delta^{18}O$ signal is dominated by ~1000 yr cyclicity during the deglaciation period whereas the carbonate record also reveals a probably solar forced ~340 yr cyclicity (Fig. 12e). Therefore, within the limitations of non-identical sampling resolution, we suggest that different drivers may underlie Sidi Ali carbonate maxima and Western Mediterranean winter rain minima (typified by $\delta^{18}O$ peaks). However, comparing the Sidi Ali $\delta^{18}O$ curve (Fig. 11f) and Sidi Ali carbonate curve (Fig. 11e), black arrows and blue bars indicate that $\delta^{18}O$ peaks (winter rain minima) are mostly in phase with centennial-scale carbonate peaks (low lake levels and/or productivity decreases). Regarding the Late Holocene, the frequency of the $\delta^{18}O$ signal (low winter rain) becomes higher (Fig. 11f) and merges into the higher-frequency Sidi Ali carbonate curve.

The Mid-Holocene change in the frequency of the Sidi Ali winter rain signal suggests a noteworthy hydro-climatic shift in the Western Mediterranean region. Here, the diminishing impact of North Atlantic meltwater discharges at the end of the Holocene deglaciation period might be a major factor (Fletcher et al., 2010; Jiang et al., 2015; Wassenburg et al., 2016). However, there is evidence for an enduring hydro-climatic shift in the entire Mediterranean region during the Mid-Holocene (Roberts et al., 2011;

Fletcher and Zielhofer, 2013; Pérez-Sanz et al., 2013; Dean et al., 2015). The decrease in summer insolation (Fig. 11d) corresponds with a southward movement of the monsoon rains at the end of the African Humid Period (deMenocal et al., 2000; Shanahan et al., 2015). Although we have no evidences yet for a direct impact of Saharan air masses on Holocene hydro-climatic variability in the Middle Atlas, the Mid-Holocene southward shift of the ITCZ might be coupled with a weakening and northward shift of the Atlantic winter storm tracks (Black et al., 2011; Kutzbach et al., 2014) leading to enduring drier winter conditions.

5.3.4. Centennial-scale hydro-climatic variability during the Late Holocene

For the Late Holocene, the comparison of the Sidi Ali $\delta^{18}O$ curve with the *Cedrus* pollen record shows decreased *Cedrus* abundances with aridity during phases of reduced winter rain ($\delta^{18}O$ peaks and red arrows in Fig. 9). Furthermore, the majority of Western Mediterranean winter rain minima (Fig. 11f) correspond with Sidi Ali carbonate peaks (Fig. 11e) indicating probably low lake levels during arid phases. Late Holocene Sidi Ali winter rain minima and corresponding Sidi Ali carbonate peaks seem to be in phase with centennial-scale sub-polar Atlantic warming (Fig. 11g, Jiang et al., 2015). This pattern remains consistent and is especially the case at 4.4, 3.5, 2.9, 2.2, 1.7, 1.5, 0.7, and 0.2 cal ka BP. Late Holocene Sidi Ali winter rain minima and Atlantic warming (Jiang et al., 2015) are probably paced by solar maxima (Fig. 11a). Overall, we observe a probable coincidence of Western Mediterranean winter rain minima with Atlantic warming and winter rain maxima with Atlantic cooling and solar minima. This is in contrast to the hydro-climatic Atlantic forcing mechanism during the Early Holocene. With no major ice-sheets remaining, the Late Holocene linkage may represent an overall similar Atlantic situation to modern. Whereas the Early Holocene *cold relapses* (Wanner et al., 2015) with winter rain minima are probably associated with meltwater discharges the Late Holocene cold episodes with winter rain maxima might reflect coupled atmosphere-ocean variability including subtropical gyre strength changes (Moffa-Sánchez et al., 2014) probably paced by centennial-scale solar minima (Fig. 11a, e.g. 3.3, 2.7, 1.8, 1.2, 0.4 cal ka BP).

5.3.5. North Atlantic Oscillation (NAO)

The Middle Atlas is one of the key regions for the reconstruction of past NAO variability (Wassenburg et al., 2016). Our study suggests a synchronism of Late Holocene Atlantic cooling and winter rain maxima in the Western Mediterranean at sub-millennial to centennial timescales. Hence, we might deduce negative NAO-like conditions during Atlantic cooling, which are associated with enhanced precipitation over the Western Mediterranean. This is in agreement with Martín-Puertas et al. (2008), Trouet et al. (2009) and Olsen et al. (2012), who postulate sub-millennial- to centennial-scale negative NAO stages during Atlantic cooling. Furthermore, Late Holocene winter rain maxima and Atlantic cooling events generally correspond with reduced solar activity (Fig. 11a, Steinhilber et al., 2009). This is in phase with present-day NAO pattern, which reveals predominantly negative NAO modes during solar minima (Matthes, 2011).

Furthermore, the Late Holocene fluctuations in Atlantic warming and winter rain minima might correspond with cyclic changes in Western Mediterranean storm activity, pointing to centennial dynamics linked with large-scale atmospheric circulation changes (Sabatier et al., 2012; Degeai et al., 2015). However, age uncertainties between the different records do not allow a clear synchronicity.

5.3.6. Atlantic cooling events and Western Mediterranean winter rain minima

In summary, we are able to derive two hydro-climatic models of Western Mediterranean winter rain minima that reveal contrasting North Atlantic forcing mechanisms:

I) During the Early Holocene, winter rain minima occured during Atlantic cooling events (Fig. 13a). Low Sidi Ali lake levels and high $\delta^{18}O$ values indicate reduced winter rain in the Middle Atlas. Parallels with the Western Mediterranean lowlands and contrasting signals of enhanced flooding and high lake levels in Central Europe reveal a more northern track of mid-latitude westerlies. In the Middle Atlas, Early Holocene Atlantic cooling corresponds with a possible enhancement of spring precipitation, reduced evaporation, and a resulting increase in moisture during the growing season with reduced fire activity and peaks in *Cedrus* pollen. In contrast, the lowland Western Mediterranean forest declines point to hydrological stress and more aridity. During Early Holocene Atlantic warming (Fig. 13b) low $\delta^{18}O$ values indicate enhanced winter rainfall in the Western Mediterranean with high Sidi Ali lake levels. Warm temperatures during the growing season do not favour the cold and humid taxon *Cedrus*, and summer drought effects on vegetation are strong in the Middle Atlas. In contrast, the Western Mediterranean lowlands reveal a dense forest cover due to reduced hydrological stress.

II) During the Late Holocene, winter rain maxima occur during Atlantic cooling events (Fig. 13c). High Sidi Ali lake levels and low $\delta^{18}O$ values indicate enhanced winter rain in the Middle Atlas. Parallels with the Western Mediterranean lowlands reveal a southern and meridional track of mid-latitude westerlies that corresponds with the modern hydro-climatic pattern of a negative NAO mode. In the Middle Atlas, Late Holocene Atlantic cooling coincides with reduced fire activity and peaks in *Cedrus* pollen. During Late Holocene Atlantic warming (Fig. 13d) high $\delta^{18}O$ values indicate reduced winter rainfall in the Western Mediterranean with low Sidi Ali lake levels. Reduced precipitation and warm temperatures during the growing season do not favour the cold and humid taxon *Cedrus*. Summer drought effects on vegetation are strong in the Middle Atlas and in the Western Mediterranean lowlands.

6. Conclusions

A new drilling at Lake Sidi Ali at the deepest part of the basin has produced a 19.63 m sequence of homogenous silty organic sediments corresponding to the last 12,000 yr, indicating very high long-term sedimentation rates (of ~1.6 mm/yr). These provide the opportunity for multi-proxy palaeolimnological investigation at sub-centennial temporal resolution. New radiocarbon data confirm a reservoir effect up to ~950 yr. In order to circumvent this problem we apply a systematic dating of pollen concentrates and a Bayesian age model approach to generate the most robust site chronology yet for a Holocene lake record in NW Africa.

Our data confirm the high hydro-climatic sensitivity of Middle Atlas lakes towards climatic changes in the Western Mediterranean and the large-scale North Atlantic realm as highlighted in previous studies (e.g. Lamb et al., 1995, 1999; Cheddadi et al., 1998; Nourelbait et al., 2014, 2015; Tabel et al., 2016). Improved ^{14}C pollen dating techniques provide for the first time a robust sub-millennial-scale to centennial-scale chronostratigraphy from Mediterranean North Africa that allows a high-resolution reconstruction of abrupt millennial- to centennial-scale climatic changes

a) Early Holocene

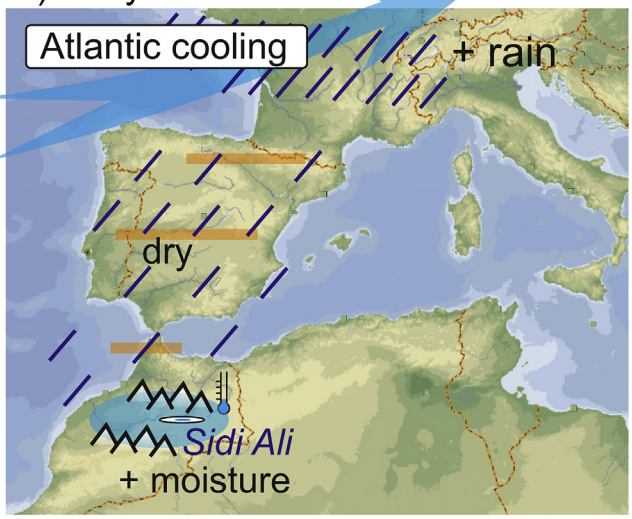

	Temperature	Humidity
Sub-polar North Atlantic	-	
Central Europe	-	+ (winter)
W Mediterranean lowlands	-	-
Sidi Ali catchment	-	+ (spring)
E Mediterranean lowlands	-	-
Sidi Ali lake level	↓	

b) Early Holocene

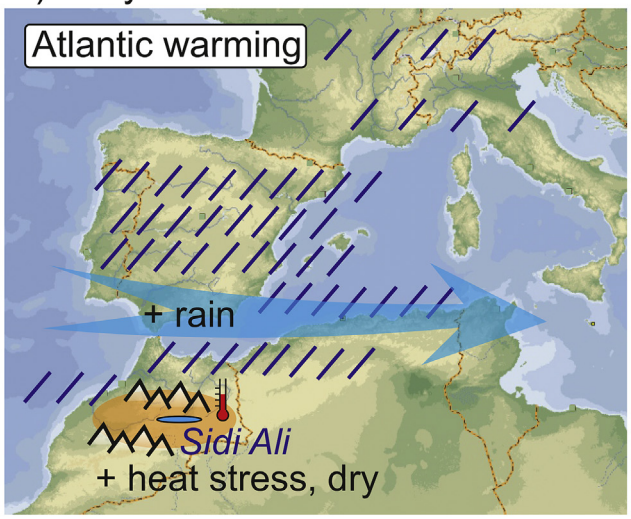

	Temperature	Humidity
Sub-polar North Atlantic	+	
Central Europe	+	- (winter)
W Mediterranean lowlands	+	+
Sidi Ali catchment	++	- (spring)
E Mediterranean lowlands	+	+
Sidi Ali lake level	↑	

c) Late Holocene (negative NAO)

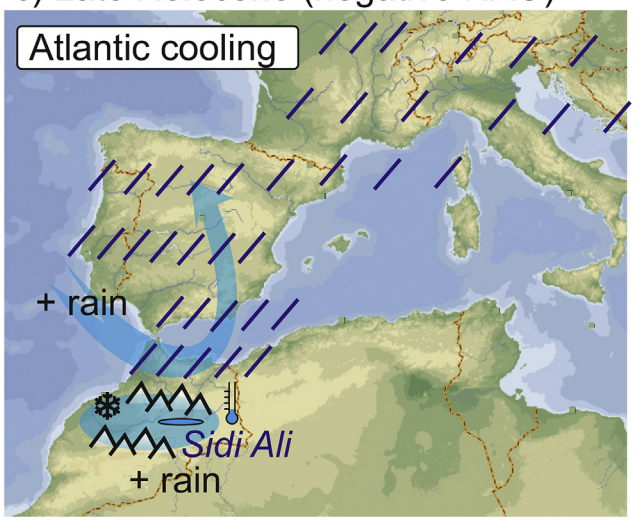

	Temperature	Humidity
Sub-polar North Atlantic	-	
Northern Europe	- (winter)	- (winter)
W Mediterranean lowlands	-	+ (winter, spring)
Sidi Ali catchment	-	+ (winter, spring)
E Mediterranean lowlands	-	
Sidi Ali lake level	↑	

d) Late Holocene (positive NAO)

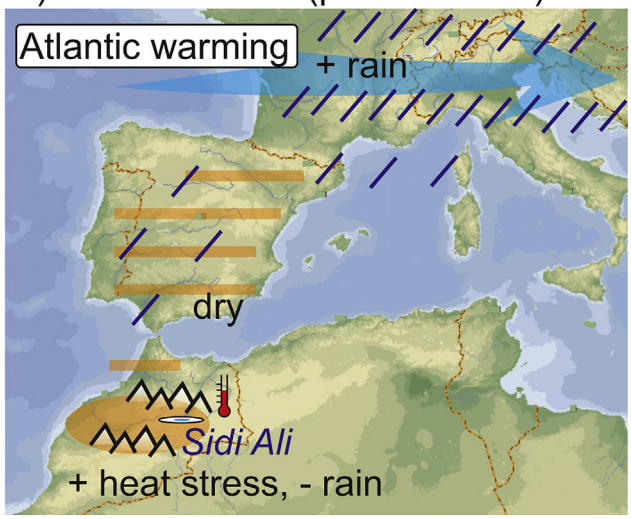

	Temperature	Humidity
Sub-polar North Atlantic	+	
Northern Europe	+ (winter)	+ (winter)
W Mediterranean lowlands	+	-- (winter, spring)
Sidi Ali catchment	++	-- (winter, spring)
E Mediterranean lowlands	+	
Sidi Ali lake level	↓	

Fig. 13. Hydro-climatic models for the Western Mediterranean region. a) Early Holocene Atlantic cooling with winter rain minima, b) Early Holocene Atlantic warming with winter rain maxima, c) Late Holocene Atlantic cooling with winter rain maxima, and d) Late Holocene Atlantic warming with winter rain minima.

during the last 12,000 years.

Lake internal proxies reveal a series of long-term changes corresponding to changes in lake productivity and lake level. These changes are likely to be driven by progressive climate changes across the YD-Holocene boundary and throughout the Holocene, and by anthropogenic impact in the catchment in the last ~1400 years. A low lake level during the YD is followed by high lake levels during the Early Holocene. After a long-lasting phase of low lake level between 6.6 and 5.4 cal ka BP the lake level rose again, and finally decreased towards the Late Holocene. In Mediterranean environments lake level lowering indicates changes in the precipitation/evaporation (P/E) ratio.

A long-term stable O isotope trend is consistent with wider trends towards drier conditions (e.g. W Mediterranean aridification, end of the AHP). However, a drying trend is not consistent with biotic (e.g. pollen records of *Cedrus* expansion) signals in the Middle Atlas, and an alternative interpretation of the isotopes, namely a shift from winter to spring precipitation with a probable shift in prevailing moisture sources must be considered. Here, the warm Early Holocene is dominated by Atlantic winter precipitation whereas the cool Late Holocene features relatively more spring rains from Mediterranean origin. This interpretation of shifts in circulation pattern may also apply to sub-millennial-scale fluctuations in the isotopes during the Early Holocene. The Middle Atlas trend contrasts with the Holocene hydro-climatic situation in the thermo-Mediterranean lowlands: a warm Early Holocene with rather dry bioclimatic conditions in the Middle Atlas corresponds with a maximum in temperate and Mediterranean forest occupation in the lowlands. Hence, a contrasting relative importance of winter precipitation and summer temperature/drought stress is inferred.

The Sidi Ali record shows recurrent sub-millennial- to centennial-scale lake lowering and decreases in Western Mediterranean winter rain at 11.4, 10.3, 9.2, 8.2, 7.2, 6.6, 6.0, 5.4, 5.0, 4.4, 3.5, 2.9, 2.2, 1.9, 1.7, 1.5, 1.0, 0.7, and 0.2 cal ka BP. Intriguingly, decreases in Western Mediterranean winter precipitation ($\delta^{18}O$ increases) correspond with low lake levels (Sidi Ali carbonate peaks), but in contrast, higher frequency centennial-scale Sidi Ali carbonate peaks (grey bars in Fig. 11) do not coincide necessarily with winter rain minima. Although this contrast must be further tested against higher resolution isotope measurements, we hypothesise different but interacting drivers for Sidi Ali carbonate peaks and Western Mediterranean winter rain minima, for example with local temperature impacts on carbonate precipitation and supra-regional precipitation regime impacts on oxygen isotopes.

In terms of forcing factors, the new multiproxy dataset from Lake Sidi Ali presents strong indications of pervasive solar forcing at the Western Mediterranean – Saharan margin. Specifically, long term modulation of Sidi Ali lake level by the Hallstatt cycle, Early Holocene dominance of millennial-scale variability associated with the Eddy cycle, and a mid-Holocene shift towards prevailing centennial-scale fluctuations on timescales of ~340 yr and ~200 yr all match closely with solar signals (e.g. Steinhilber et al., 2012).

Solar signals are likely to impact on the Middle Atlas via modulation of Atlantic climate variability. During the Early Holocene, winter rain minima and local cooling are in phase with abrupt cooling events in the (sub-)polar North Atlantic (Rasmussen et al., 2007; Jiang et al., 2015). Early Holocene Atlantic cooling and corresponding Western Mediterranean winter rain minima were probably associated with meltwater discharges and weakening of the Atlantic overturning circulation. In contrast, our proxy parameters do not show so far a clear impact of Saharan air masses on Mediterranean hydro-climate in North Africa. However, corresponding to the end of the African Humid Period at ~5 ka, there is a mid-Holocene switch in phasing between Atlantic cooling and Western Mediterranean humidity. There is evidence for an enduring hydro-climatic change in the overall Atlantic atmosphere-ocean system and the response to external forcing. In contrast to the Early Holocene, Late Holocene Atlantic cooling coincides with Western Mediterranean humid winters. The Late Holocene hydro-climatic system with simultaneous winter rain maxima, Atlantic cooling and solar minima is in phase with present-day/historical NAO pattern, which predominantly reveals increases in winter rain (negative NAO) during solar minima.

Acknowledgements

Christoph Zielhofer, Steffen Mischke and William Fletcher as principal investigators thank the German Research Foundation (DFG, ZI 721/9-1) and the Natural Environment Research Council (New Investigator Award to W Fletcher, NE/K000608/1, and NERC RCF dating awards, 1765.1013 and 1809.0414) for generous funding of the fieldwork and lab analyses. The authors are grateful to the Institut National des Sciences de l'Archéologie et du Patrimoine (INSAP, Rabat), the Centre National d'Hydrobiologie et de Pisciculture (CNHP, Azrou) and to the Caidad d'Azrou for helpful support in field and in preparing the expedition in autumn 2012. Acknowledgements to Mustapha Rhanem for assistance in obtaining the Sidi Ali meteorological data. Hanno Meyer of the stable isotope laboratory at AWI Potsdam is highly acknowledged for providing the stable water isotope data. Finally, the authors are grateful to two anonymous reviewers for helpful comments and suggestions.

Appendix A. Supplementary data

Supplementary data related to this article can be found at http://dx.doi.org/10.1016/j.quascirev.2016.11.037.

References

Anderson, J., et al., 2015. European Diatom Database (2015). http://craticula.ncl.ac.uk/Eddi/jsp/index.jsp [5.10.2015].

Appleby, P.G., Nolan, P.J., Gifford, D.W., Godfrey, M.J., Oldfield, F., Anderson, N.J., Battarbee, R.W., 1986. ^{210}Pb dating by low background gamma counting. Hydrobiologia 141, 21–27.

Appleby, P.G., Richardson, N., Nolan, P.J., 1992. Self-absorption corrections for well-type germanium detectors. Nucl. Instrum. Methods B 71, 228–233.

Barker, P.A., Roberts, N., Lamb, H.F., van der Kaars, S., Benkaddour, A., 1994. Interpretation of Holocene lake-level change from diatom assemblages in Lake Sidi Ali, Middle Atlas, Morocco. J. Paleolimnol. 12, 223–234.

Bartolomé, M., Moreno, A., Sancho, C., Stoll, H.M., Cacho, I., Spötl, C., Belmonte, A., Edwards, R.L., Cheng, H., Hellstrom, J.C., 2015. Hydrological change in Southern Europe responding to increasing North Atlantic overturning during Greenland Stadial 1. Proc. Natl. Acad. Sci. 112 (21), 6568–6572.

Benito, G., Macklin, M.G., Zielhofer, C., Jones, A.F., Machado, M.J., 2015. Holocene flooding and climate change in the Mediterranean. Catena 130, 13–33.

Benkaddour, A., Lamb, H., Leng, M., Gasse, F., 2005. Stable Isotope Records of Holocene Environmental Change from Moroccan Lakes: an Emerging Synthesis. http://www.pages-igbp.org/download/docs/meeting-products/posters/2005-osm2/Benkaddour-A.pdf [26.01.2015].

Berger, A., 1978. Long-term variations of caloric insolation resulting from the earth's orbital elements. Quat. Res. 9, 139–167.

Black, E., Brayshaw, D., Black, S., Rambeau, C., 2011. Using proxy data, historical climate data and climate models to investigate aridification during the Holocene. In: Mithen, S., Black, E. (Eds.), Water, Life and Civilisation. Cambridge University Press, Cambridge, pp. 105–112.

Bond, G., Kromer, B., Beer, J., Muscheler, R., Evans, M.N., Showers, W., Hoffmann, S., Lotti-Bond, R., 2001. Persistent solar influence on North Atlantic climate during the Holocene. Science 294, 2130–2136.

Born, K., Fink, A., Paeth, H., 2008. Dry and wet periods in the northwestern Maghreb for present day and future climate conditions. Meteorol. Z. 17, 533–551.

Bosmans, J.H.C., Drijfhout, S.S., Tuenter, E., Hilgen, F.J., Lourens, L.J., Rohling, E.J., 2015. Precession and obliquity forcing of the freshwater budget over the Mediterranean. Quat. Sci. Rev. 123, 16–30.

Bout-Roumazeilles, V., Combourieu-Nebout, N., Desprat, S., Siani, G., Turon, J.L., Essallami, L., 2013. Tracking atmospheric and riverine terrigenous supplies variability during the last glacial and the Holocene in central Mediterranean. Clim. Past 9, 1065–1087.

Bronk Ramsey, C., 2008. Deposition models for chronological records. Quat. Sci. Rev.

27, 42–60.
Bronk Ramsey, C., 2009a. Bayesian analysis of radiocarbon dates. Radiocarbon 51, 337–360.
Bronk Ramsey, C., 2009b. Dealing with outliers and offsets in radiocarbon dating. Radiocarbon 51, 1023–1045.
Bronk Ramsey, C., Lee, S., 2013. Recent and planned developments of the program OxCal. Radiocarbon 55, 720–730.
Cacho, I., Grimalt, J.O., Canals, M., Sbaffi, L., Shackleton, N.J., Schönfeld, J., Zahn, R., 2001. Variability of the Western Mediterranean sea surface temperature during the last 25,000 years and its connection with the Northern Hemisphere climatic changes. Paleoceanography 16, 40–52.
Carrión, J.S., 2002. Patterns and processes of Late Quaternary environmental change in a montane region of southwestern Europe. Quat. Sci. Rev. 21, 2047–2066.
Carrión, J.S., Sánchez-Gómez, P., Mota, J.F., Yll, R., Chaín, C., 2003. Holocene vegetation dynamics, fire and grazing in the Sierra de Gádor, southern Spain. Holocene 13, 839–849.
Celle-Jeanton, H., Zouari, K., Travi, Y., Daoud, A., 2001. Caractérisation isotopique des pluies en Tunisie. Essai de typologie dans la région de Sfax. Comptes Rendus de l'Académie des Sci. - Ser. IIA - Earth Planet. Sci. 333, 625–631.
Cheddadi, R., Lamb, H.F., Guiot, J., van der Kaars, S., 1998. Holocene climatic change in Morocco: a quantitative reconstruction from pollen data. Clim. Dyn. 14, 883–890.
Cheddadi, R., Nourelbait, M., Bouaissa, O., Tabel, J., Rhoujjati, A., López-Sáez, J.A., Alba-Sánchez, F., Khater, C., Ballouche, A., Dezileau, L., Lamb, H., 2015. A history of human impact on Moroccan Mountain landscapes. Afr. Archaeol. Rev. 32, 233–248.
Corella, J.P., Benito, G., Rodriguez-Lloveras, X., Brauer, A., Valero-Garcés, B.L., 2014. Annually-resolved lake record of extreme hydro-meteorological events since AD 1347 in NE Iberian Peninsula. Quat. Sci. Rev. 93, 77–90.
Croudace, I.W., Rindby, A., Rothwell, R.G., 2006. ITRAX: description and evaluation of a new multi-function X-ray core scanner. Geol. Soc. Lond. Spec. Publ. 267, 51–63.
Dean, J.R., Jones, M.D., Leng, M.J., Noble, S.R., Metcalfe, S.E., Sloane, H.J., Sahy, D., Eastwood, W.J., Roberts, C.N., 2015. Eastern Mediterranean hydroclimate over the late glacial and Holocene, reconstructed from the sediments of Nar lake, central Turkey, using stable isotopes and carbonate mineralogy. Quat. Sci. Rev. 124, 162–174.
Degeai, J.P., Devillers, B., Dezileau, L., Oueslati, H., Bony, G., 2015. Major storm periods and climate forcing in the Western Mediterranean during the Late Holocene. Quat. Sci. Rev. 129, 37–56.
deMenocal, P.B., Ortiz, J., Guilderson, T., Adkins, J., Sarnthein, M., Baker, L., Yarusinsky, M., 2000. Abrupt onset and termination of the African Humid Period: rapid climatic responses to gradual insolation forcing. Quat. Sci. Rev. 19, 347–361.
Diffenbaugh, N.S., Pal, J.S., Giorgi, F., Gao, X., 2007. Heat stress intensification in the Mediterranean climate change hotspot. Geophys. Res. Lett. 34, L11706.
Duan, F., Wang, Y., Shen, C.C., Wang, Y., Cheng, H., Wu, C.C., Hu, H.M., Kong, X., Liu, D., Zhao, K., 2014. Evidence for solar cycles in a late Holocene speleothem record from Dongge Cave, China. Sci. Rep. 4 http://dx.doi.org/10.1038/srep05159.
El Hamouti, N., 1991. Changements hydroclimatiques abrupts dans le Moyen Atlas marocain depuis le Dernier Maximum Glaciaire. C. R. Acad. Sci. Série II 313, 259–265.
El Hamouti, N., 2003. Changements hydrologiques et climatiques dans le Moyen Atlas marocain depuis 18 Ka BP à partir de l'étude des diatomées du site de Tigalmamine. Doctorat ès Sciences de l'Université Mohamed I, p. 300.
El Hamouti, N., 2014. Climatic and hydrologic changes in Moroccan Middle Atlas during the Holocene. In: Fernández-Montes, S., Rodrigo, F.S. (Eds.), Cambio Climático Y Cambio Global. Publicaciones de la Asociación Española de Climatología Serie A, pp. 709–716.
Flato, G., et al., 2013. Evaluation of climate models. In: Stocker, T.F., et al. (Eds.), Climate Change 2013: the Physical Science Basis. Contribution of Working Group I to the Fifth Assessment Report of the Intergovernmental Panel on Climate Change. Cambridge University Press, Cambridge, pp. 741–866.
Fletcher, W.J., Sánchez Goñi, M.F., 2008. Orbital- and sub-orbital-scale climate impacts on vegetation of the Western Mediterranean basin over the last 48,000 yr. Quat. Res. 70, 451–464.
Fletcher, W.J., Zielhofer, C., 2013. Fragility of Western Mediterranean landscapes during Holocene rapid climate changes. Catena 103, 16–29.
Fletcher, W.J., Sanchez Goñi, M.F., Peyron, O., Dormoy, I., 2010. Abrupt climate changes of the last deglaciation detected in a Western Mediterranean forest record. Clim. Past 6, 245–264.
Fletcher, W.J., Debret, M., Sanchez Goñi, M.F., 2013. Mid-Holocene emergence of a low-frequency millennial oscillation in western Mediterranean climate: implications for past dynamics of the North Atlantic atmospheric westerlies. Holocene 23, 153–166.
Fletcher, W.J., Zielhofer, C., Mischke, S., Campbell, J.E., Bryant, C., Xu, X., Fink, D., 2016. AMS radiocarbon dating of pollen concentrates in a karstic lake system. Quat. Geochronol. (in press).
Flower, R.J., Stevenson, A.C., Dearing, J.A., Foster, I.D.L., Airey, A., Rippey, B., Wilson, J.R.E., Appleby, P.G., 1989. Catchment disturbance inferred from palaeolimnological studies of three contrasted sub-humid environments in Morocco. J. Palaeolimnology 1, 293–322.
Friedman, I., O'Neil, J.R., 1977. Compilation of stable isotope fractionation factors of geochemical interest. In: Data of Geochemistry 6th Edition, Geological Survey Professional Paper 440–KK, p. 61.
Gasse, F., Juggins, S., Ben Khelifa, L., 1995. Diatom-based transfer functions for interring past hydrochemical characteristics of African lakes. Palaeogeogr. Palaeoclimatol. Palaeoecol. 117, 31–54.
Giorgi, F., 2006. Climate change hotspots. Geophys. Res. Lett. 33, L08707.
Heiri, O., Tinner, W., Lotter, A.F., 2004. Evidence for cooler European summers during periods of changing meltwater flux to the North Atlantic. Proc. Natl. Acad. Sci. 101, 15285–15288.
Hoffmann, T., Lang, A., Dikau, R., 2008. Holocene river activity: analysing ^{14}C-dated fluvial and colluvial sediments from Germany. Quat. Sci. Rev. 27, 2031–2040.
Hou, J., Huang, Y., Shuman, B.N., Oswald, W.W., Foster, D.R., 2012. Abrupt cooling repeatedly punctuated early-Holocene climate in eastern North America. Holocene 22, 525–529.
Hughes, P.D., Fenton, C.R., Gibbard, P.L., 2011. Quaternary glaciations of the Atlas Mountains, North Africa. In: Ehlers, J., Gibbard, P.L., Hughes, P.D. (Eds.), Developments in Quaternary Science 15. Elsevier, Amsterdam, pp. 1065–1074.
Jiang, H., Muscheler, R., Björck, S., Seidenkrantz, M.S., Olsen, J., Sha, L., Sjolte, J., Eiríksson, J., Ran, L., Knudsen, K.L., Knudsen, M., 2015. Solar forcing of Holocene summer sea-surface temperatures in the northern North Atlantic. Geology 43, 203–206.
Jones, B., Manning, D.A.C., 1994. Comparison of geochemical indices used for the interpretation of palaeoredox conditions in ancient mudstones. Chem. Geol. 111, 111–129.
Knippertz, P., Christoph, M., Speth, P., 2003. Long-term precipitation variability in Morocco and the link to the large-scale circulation in recent and future climates. Meteorol. Atmos. Phys. 83, 67–88.
Kutzbach, J.E., Chen, G., Cheng, H., Edwards, R.L., Liu, Z., 2014. Potential role of winter rainfall in explaining increased moisture in the Mediterranean and Middle East during periods of maximum orbitally-forced insolation seasonality. Clim. Dyn. 42, 1079–1095.
Krammer, K., Lange-Bertalot, H., 1991. Stillwasserflora von Mitteleuropa. Bacillariophyceae Teil 3: Centrales, Fragilariaceae, Eunotiaceae. Fischer, Stuttgart, p. 576.
Kylander, M.E., Ampel, L., Wohlfarth, B., Veres, D., 2011. High-resolution X-ray fluorescence core scanning analysis of Les Echets (France) sedimentary sequence: new insights from chemical proxies. J. Quat. Sci. 26, 109–117.
Lamb, H., van der Kaars, S., 1995. Vegetational response to Holocene climatic change: pollen and palaeolimnological data from the Middle Atlas, Morocco. Holocene 5, 400–408.
Lamb, H.F., Gasse, F., Benkaddour, A., El Hamouti, N., van der Kaars, S., Perkins, W.T., Pearce, N.J., Roberts, C.N., 1995. Relation between century-scale Holocene arid intervals in tropical and temperate zones. Nature 373, 134–137.
Lamb, H.F., Roberts, C.N., Leng, M., Barker, P.A., Benkaddour, A., Van der Kaars, S., 1999. Lake evolution in a semi-arid montane environment: responses to catchment change and hydroclimatic variation. J. Paleolimnol. 21, 325–343.
Lang, B., Bedford, A., Brooks, S.J., Jones, R.T., Richardson, N., Birks, H.J.B., Marshall, J.D., 2010. Early-Holocene temperature variability inferred from chironomid assemblages at Hawes Water, northwest England. Holocene 20, 943–954.
Leng, M.J., Marshall, J.D., 2004. Palaeoclimate interpretation of stable isotope data from lake sediment archives. Quat. Sci. Rev. 23, 811–831.
Lespez, L., Glais, A., Lopez-Saez, J.A., Le Drezen, Y., Tsirtsoni, Z., Davidson, R., Biree, L., Malamidou, D., 2016. Middle Holocene rapid environmental changes and human adaptation in Greece. Quat. Res. http://dx.doi.org/10.1016/j.yqres.2016.02.002.
Linstädter, A., Zielhofer, C., 2010. Regional fire history shows abrupt responses of Mediterranean ecosystems to centennial-scale climate change (*Olea-Pistacia* woodlands, NE Morocco). J. Arid Environ. 74, 101–110.
Linstädter, A., Baumann, G., 2013. Abiotic and biotic recovery pathways of arid rangelands: lessons from the High Atlas Mountains, Morocco. Catena 103, 3–15.
Lucchini, F., Dinelli, E., Calanchi, N., 2003. Chemostratigraphy of Lago Albano sediments (Central Italy): geochemical evidence of palaeoenvironmental changes in late Quaternary. J. Paleolimnol. 29, 109–122.
Magny, M., 2004. Holocene climate variability as reflected by mid-European lake-level fluctuations and its probable impact on prehistoric human settlements. Quat. Int. 113, 65–79.
Magny, M., Peyron, O., Sadori, L., Ortu, E., Zanchetta, G., Vannière, B., Tinner, W., 2012. Contrasting patterns of precipitation seasonality during the Holocene in the south- and northcentral Mediterranean. J. Quat. Sci. 27, 290–296.
Martín-Puertas, C., Valero-Garcés, B.L., Mata, M.P., González-Sampériz, P., Bao, R., Moreno, A., Stefanova, V., 2008. Arid and humid phases in southern Spain during the last 4000 years: the Zonar Lake record, Cordoba. Holocene 18, 907–921.
Matthes, K., 2011. Atmospheric science: solar cycle and climate predictions. Nat. Geosci. 4, 735–736.
Mayewski, P.A., Rohling, E.E., Stager, J.C., Karlén, W., Maasch, K.A., Meeker, L.D., Meyerson, E.A., Gasse, F., van Kreveld, S., Holmgren, K., Lee-Thorp, J., Rosqvist, G., Rack, F., Staubwasser, M., Schneider, R.R., Steig, E.J., 2004. Holocene climate variability. Quat. Res. 62, 243–255.
McGregor, H.V., Dupont, L., Stuut, J.-B.W., Kuhlmann, H., 2009. Vegetation change, goats, and religion: a 2000-year history of land use in southern Morocco. Quat. Sci. Rev. 28, 1434–1448.
Meisch, C., 2000. Freshwater Ostracoda of Western and Central Europe. Spektrum, Heidelberg, p. 522.
Meyer, H., Schönicke, L., Wand, U., Hubberten, H.-W., Friedrichsen, H., 2000. Isotope

studies of hydrogen and oxygen in ground ice - experiences with the equilibration technique. Isot. Environ. Health Stud. 36, 133–149.
Meyer, I., Davies, G.R., Vogt, C., Kuhlmann, H., Stuut, J.B.W., 2013. Changing rainfall patterns in NW Africa since the Younger Dryas. Aeolian Res. 10, 111–123.
Meyers, P.A., Teranes, J.L., 2001. Sediment organic matter. In: Last, W.M., Meyers, P.A., Teranes, J.L. (Eds.), Tracking Environmental Change Using Lake Sediments: Physical and Geochemical Methods, vol. 2. Kluwer, Dordrecht, pp. 239–265.
Moffa-Sánchez, P., Born, A., Hall, I.R., Thornalley, D.J., Barker, S., 2014. Solar forcing of North Atlantic surface temperature and salinity over the past millennium. Nat. Geosci. 7, 275–278.
Moore, P.D., Webb, J.A., Collison, M.E., 1991. Pollen Analysis. Blackwell, Oxford, p. 216.
Moreno, A., Svensson, A., Brooks, S.J., Connor, S., Engels, S., Fletcher, W., Genty, D., Heiri, O., Labuhn, I., Persoiu, A., Peyron, O., Sadori, L., Valero-Garcés, Wulf, S., Zanchetta, G., 2014a. A compilation of Western European terrestrial records 60-8 ka BP: towards an understanding of latitudinal climatic gradients. Quat. Sci. Rev. 106, 167–185.
Moreno, A., Sancho, C., Bartolomé, M., Oliva-Urcia, B., Delgado-Huertas, A., Estrela, M.J., Corell, D., López-Moreno, J.I., Cacho, I., 2014b. Climate controls on rainfall isotopes and their effects on cave drip water and speleothem growth: the case of Molinos cave (Teruel, NE Spain). Clim. Dyn. 43, 221–241.
Nakagawa, T., Brugiapaglia, E., Digerfeld, G., Reille, M., De Beaulieu, J.L., Yasuda, Y., 1998. Dense-media separation as a more efficient pollen extraction method for use with organic sediment/deposit samples: comparison with the conventional method. Boreas 27, 15–24.
Nourelbait, M., Rhoujjati, A., Eynaud, F., Benkaddour, A., Dezileau, L., Wainer, K., Goslar, T., Khater, C., Tabel, J., Cheddadi, R., 2014. An 18 000-year pollen and sedimentary record from the cedar forests of the Middle Atlas, Morocco. J. Quat. Sci. 29, 423–432.
Nourelbait, M., Rhoujjati, A., Benkaddour, A., Carré, M., Eynaud, F., Martinez, P., Cheddadi, R., 2015. Climate change and ecosystems dynamics over the last 6000 years in the Middle Atlas, Morocco. Clim. Past 12, 1029–1042.
Olsen, J., Anderson, N.J., Knudsen, M.F., 2012. Variability of the North Atlantic Oscillation over the past 5,200 years. Nat. Geosci. 5, 808–812.
Ojala, A.E.K., Launonen, I., Holmström, L., Tiljander, M., 2015. Effects of solar forcing and North Atlantic oscillation on the climate of continental Scandinavia during the Holocene. Quat. Sci. Rev. 112, 153–171.
Ouda, B., El Hamdaoui, A., Ibn Majah, M., 2005. Isotopic composition of precipitation at three Moroccan stations influenced by oceanic and Mediterranean air masses. In: Isotopic Composition of Precipitation in the Mediterranean Basin in Relation to Air Circulation Patterns and Climate. IAEA, Vienna, pp. 125–140.
Pérez-Sanz, A., González-Sampériz, P., Moreno, A., Valero-Garcés, B., Gil-Romera, G., Rieradevall, M., Tarrats, P., Lasheras-Álvarez, L., Morellón, M., Belmonte, A., Sancho, C., Sevilla-Callejo, M., Navas, A., 2013. Holocene climate variability, vegetation dynamics and fire regime in the central Pyrenees: the Basa de la Mora sequence (NE Spain). Quat. Sci. Rev. 73, 149–169.
Rach, O., Brauer, A., Wilkes, H., Sachse, D., 2014. Delayed hydrological response to Greenland cooling at the onset of the Younger Dryas in western Europe. Nat. Geosci. 7, 109–112.
Rasmussen, S.O., Vinther, B.M., Clausen, H.B., Andersen, K.K., 2007. Early Holocene climate oscillations recorded in three Greenland ice cores. Quat. Sci. Rev. 26, 1907–1914.
Reddad, H., Etabaai, I., Rhoujjati, A., Taieb, M., Thevenon, F., Damnati, B., 2013. Fire activity in North West Africa during the last 30,000 cal years BP inferred from a charcoal record from Lake Ifrah (Middle Atlas–Morocco): climatic implications. J. Afr. Earth Sci. 84, 47–53.
Reimer, P.J., et al., 2013. IntCal13 and MARINE13 radiocarbon age calibration curves 0-50000 years calBP. Radiocarbon 55, 1869–1887.
Roberts, N., Jones, M.D., Benkaddour, A., Eastwood, W.J., Filippi, M.L., Frogley, M.R., Lamb, H.F., Leng, M.J., Reed, J.M., Stein, M., Stevens, L., Valero-Garces, B., Zanchetta, G., 2008. Stable isotope records of Late Quaternary climate and hydrology from Mediterranean lakes: the ISOMED synthesis. Quat. Sci. Rev. 27, 2426–2441.
Roberts, N., Brayshaw, D., Kuzucuoglu, C., Perez, R., Sadori, L., 2011. The mid-Holocene climatic transition in the Mediterranean: causes and consequences. Holocene 21, 3–14.
Saadi, M., Hilali, E.A., Bensaïd, M., Boudda, A., Dahmani, M., 1985. Carte Géologique du Maroc 1/1,000,000. Notes et Mémoires 260. Editions du Service Géologique du Maroc, Rabat.
Sabatier, P., Dezileau, L., Colin, C., Briqueu, L., Bouchette, F., Martinez, P., Siani, G., Raynal, O., Von Grafenstein, U., 2012. 7000 years of paleostorm activity in the NW Mediterranean Sea in response to Holocene climate events. Quat. Res. 77, 1–11.
Sayad, A., Chakiri, S., Martin, C., Bejjaji, Z., Echarfaoui, H., 2011. Effet des conditions climatiques sur le niveau du lac Sidi Ali (Moyen Atlas, Maroc). Physio-Géo 5, 251–268.
Schulz, M., Mudelsee, M., 2002. REDFIT: estimating red-noise spectra directly from unevenly spaced paleoclimatic time series. Comput. Geosci. 28, 421–426.
Schwalb, A., 2002. Lacustrine ostracodes as stable isotope recorders of late-glacial and Holocene environmental dynamics and climate. J. Paleolimnol. 29, 265–351.
Shanahan, T.M., McKay, N.P., Hughen, K.A., Overpeck, J.T., Otto-Bliesner, B., Heil, C.W., King, J., Scholz, C.A., Peck, J., 2015. The time-transgressive termination of the African humid period. Nat. Geosci. 8, 140–144.
Solomon, S., Plattner, G.-K., Knutti, R., Friedlingsteind, P., 2009. Irreversible climate change due to carbon dioxide emissions. Proc. Natl. Acad. Sci. 106, 1704–1709.
Soon, W., Velasco Herrera, V.M., Selvaraj, K., Traversi, R., Usoskin, I., Chen, C.T.A., Lou, J.Y., Kao, S.J., Carter, R.M., Pipin, V., Severi, M., Becagli, S., 2014. A review of Holocene solar-linked climatic variation on centennial to millennial timescales: physical processes, interpretative frameworks and a new multiple cross-wavelet transform algorithm. Earth-Science Rev. 134, 1–15.
Steinhilber, F., Beer, F., Frohlich, C., 2009. Total solar irradiance during the Holocene. Geophys. Res. Lett. 36, L 19704.
Steinhilber, F., Abreu, J.A., Beer, J., Brunner, I., Christl, M., Fischer, H., Heikkilä, U., Kubik, P.W., Mann, M., McCracken, K.G., Miller, H., 2012. 9,400 years of cosmic radiation and solar activity from ice cores and tree rings. Proc. Natl. Acad. Sci. 109, 5967–5971.
Tabel, J., Khater, C., Rhoujjati, A., Dezileau, L., Bouimetarhan, I., Carre, M., Vidal, L., Benkaddour, A., Nourelbait, M., Cheddadi, R., 2016. Environmental changes over the past 25 000 years in the southern Middle Atlas, Morocco. J. Quat. Sci. http://dx.doi.org/10.1002/jqs.2841.
Talbot, M.R., 1990. A review of the palaeohydrological interpretation of carbon and oxygen isotopic ratios in primary lacustrine carbonates. Chem. Geol. 80, 261–279.
Torrence, C., Compo, G.P., 1998. Practical guide to wavelet analysis. Bull. Am. Meteorol. Soc. 79, 61–78.
Trouet, V., Esper, J., Graham, N.E., Baker, A., Scourse, J.D., Frank, D.C., 2009. Persistent positive North Atlantic Oscillation mode dominated the Medieval climate anomaly. Science 324, 78–80.
Vandergoes, M.J., Prior, C.A., 2003. AMS dating of pollen concentrates; a methodological study of late Quaternary sediments from south Westland, New Zealand. Radiocarbon 45, 479–491.
Vannière, B., Power, M.J., Roberts, N., Tinner, W., Carrión, J., Magny, M., Bartlein, P., 2011. Circum-Mediterranean fire activity and climate changes during the mid-Holocene environmental transition (8500–2500 cal yr BP). Holocene 21, 53–73.
Wanner, H., Mercolli, L., Grosjean, M., Ritz, S.P., 2015. Holocene climate variability and change; a data-based review. J. Geol. Soc. 172, 254–263.
Wassenburg, J.A., Dietrich, S., Fietzke, J., Fohlmeister, J., Jochum, K.P., Scholz, D., Richter, D.K., Sabaoui, A., Spötl, C., Lohmann, G., Andreae, M.O., Immenhauser, A., 2016. Reorganization of the North Atlantic Oscillation during early Holocene deglaciation. Nat. Geosci. 9, 602–605.
Wolf, D., Faust, D., 2015. Western Mediterranean environmental changes: evidences from fluvial archives. Quat. Sci. Rev. 122, 30–50.
Zielhofer, C., Faust, D., 2008. Mid- and Late Holocene fluvial chronology of Tunisia. Quat. Sci. Rev. 27, 580–588.
Zielhofer, C., Bussmann, J., Ibouhouten, H., Fenech, K., 2010. Flood frequencies reveal Holocene rapid climate changes (Lower Moulouya River, NE Morocco). J. Quat. Sci. 25, 700–714.